219

MIDWESTERN UNIVERSITIES RESEARCH ASSOCIATION

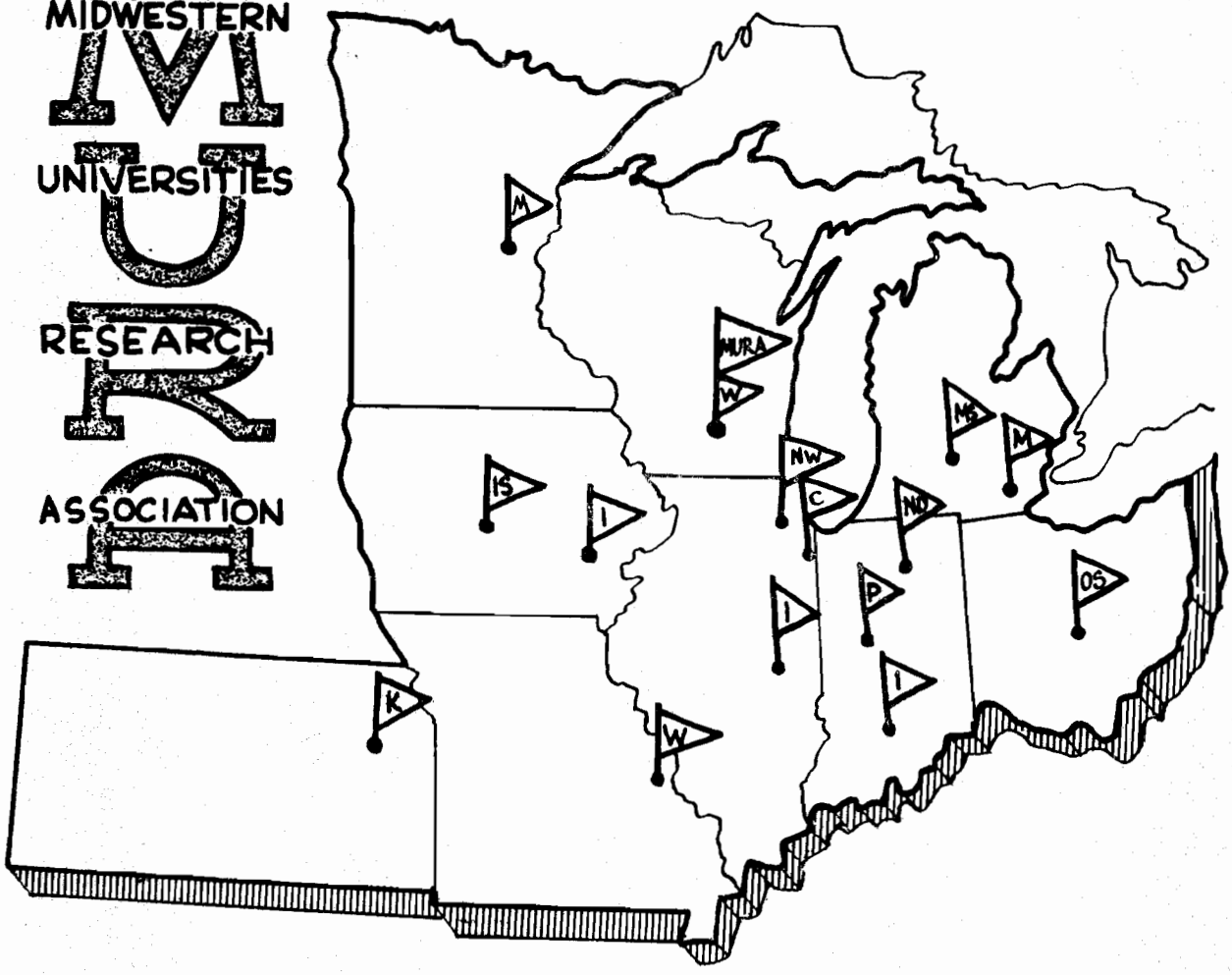

AN ELECTRON MODEL FIXED FIELD ALTERNATING GRADIENT ACCELERATOR

REPORT NUMBER 219

MURA 219

March 5, 1957

An Electron Model Fixed Field Alternating Gradient Accelerator+ (Submitted to the Review of Scientific Instruments)

F. T. Cole*, R. O. Haxby**, L. W. Jones***, C. H. Pruett and K. M. Terwilliger****

MIDWESTERN UNIVERSITIES RESEARCH ASSOCIATION
Madison, Wisconsin

ABSTRACT

A radial sector FFAG accelerator has been constructed and successfully operated. In this 8 sector accelerator electrons are betatron accelerated from 25 to 400 Kev using both continuous and pulsed injection. The number of radial betatron oscillations per revolution may be varied from 2.3 to 3 and the number of vertical oscillations per revolution from 1 to 3. Calculations of these oscillation frequencies using various approximations are described and discussed. These frequencies have been measured statically with the unaccelerated beam and dynamically using an rf perturbing voltage on the accelerated beam. Results of these calculations and experiments are in satisfactory agreement. Effects of misalignments have been measured and are in close agreement with calculations presented. A survey has been made over a large area of the betatron oscillation stability region. The effects of the many resonances observed are in good qualitative agreement with theory.

+ Work supported by the N.S.F., O.N.R. and A.E.C.

* State University of Iowa, Iowa City, Iowa

** Purdue University, Lafayette, Indiana

*** University of Michigan and Michigan Memorial Phoenix Project, Ann Arbor, Michigan

**** University of Michigan, Ann Arbor, Michigan

I. INTRODUCTION

In fixed field alternating gradient accelerators[1] (FFAG) the average guide field can increase rapidly with radius, permitting a large range of momenta in a narrow radial aperture, while the stability of radial and vertical betatron oscillations is maintained with alternating gradient focusing. FFAG accelerators are generally of the radial sector or spiral sector types, the designations referring to the geometry of the magnet edges. In radial sector accelerators the field direction reverses in successive magnets, while with spiraled sectors a much smaller field variation is required.

In order to study some of the properties of FFAG accelerators and to confirm theoretical predictions a radial sector FFAG electron model has been constructed and put into operation.[2] The following article describes the orbit theory, the accelerator design and construction, the magnetic field measurements and the static measurements of the betatron frequencies. It discusses the accelerated beam obtained with pulsed and continuous injection, and the radio frequency measurements of the betatron frequencies, and compares the experimental values with the theoretical results. The effects of field perturbations and betatron resonances on the accelerated beam are presented and discussed.

II. GENERAL DESCRIPTION AND PARAMETERS

In this machine there are sixteen magnets (eight sectors) arranged in a ring (Fig. 1) with the field direction reversed in successive magnets. Away from the fringing region the fields have a constant magnitude along an equilibrium orbit. The overall scale was chosen large enough to give adequate access to all

components, and yet small enough so that parts would be easy to construct and handle and magnetic fields would not be too low.

Betatron acceleration of the electrons is used for simplicity. The resulting accelerator injects electrons of about 25 kilovolts at a radius of 34 cm. and accelerates them in magnetic fields varying from 40 to 150 gauss to an energy of about 400 kilovolts at a radius of 50 centimeters (Fig. 2). Although more than the 8 sectors would have allowed a smaller radial aperture and larger ν values (the number of betatron oscillations per revolution), it would also have required a smaller vertical aperture and would have otherwise complicated construction.

A summary of the design parameters is given in Table I.

TABLE I. Design parameters for the FFAG electron accelerator

$N = 8$	the number of magnet pairs (sectors).
$r_1/\rho = 2.85$	the ratio of the orbit radius to the radius of curvature at the centers of positive curvature and negative curvature magnets.
$r_2/\rho = 2.59$	
$n_o = \frac{\rho}{B}\frac{\partial B}{\partial r} = 1.18$	at the center of a positive curvature magnet.
$k = \frac{r}{B}\frac{\partial B}{\partial r} = 3.36$	at every point in the machine.
$\theta_1 = 25.74^o$	the angle subtended by positive curvature magnets.
$\theta_2 = 10.44^o$	the angle subtended by negative curvature magnets.
$\theta_s = 4.41^o$	the angle subtended by "straight" sections.
$r_i = 32$ cm, $r_o = 54$ cm	the inner and outer radii of the inside of the vacuum tank.
$G_i = 4.0$ cm	the magnet gap at 32 cm radius.
G/r = constant	for all r across the useful aperture.
$Z = 2.41$ cm	the total vertical aperture available inside the vacuum tank at all radii.

III. ORBIT THEORY AND DESIGN

This section discusses the orbit theory of the present accelerator. Part A gives a general discussion of orbit theory in radial sector FFAG accelerators, with special emphasis on the equations used in the later discussion. Part B describes the calculations done in the original design to arrive at a magnet geometry. Part C describes the calculations done after the accelerator was constructed, using the more powerful methods now available.

A. Orbit Theory of Radial Sector FFAG Accelerators

If the acceleration process, which is a small effect per revolution, is neglected the problem reduces to the motion of a charged particle of constant total (relativistic) momentum p in a static magnetic field. The equations of motion of such a particle may be derived from Jacobi's form of the principle of least action,[3]

$$\delta \int_{S_1}^{S_2} \left(p + \frac{e}{c} \underline{A} \right) \cdot d\underline{S} = 0 \tag{3.1}$$

Introducing cylindrical coordinates (r, θ, ζ) and using θ as independent variable, $\dot{\underline{S}} = \frac{d\underline{S}}{d\theta}$ has components ($\dot{r}$, r, $\dot{\zeta}$). Using these, (3.1) may be written

$$\delta \int_{\theta_1}^{\theta_2} \left\{ \sqrt{r^2 + \dot{r}^2 + \dot{\zeta}^2} + \frac{e}{cp} \left[\dot{r} A_r + r A_\theta + \dot{\zeta} A_\zeta \right] \right\} d\theta = 0 \tag{3.2}$$

and the equations of motion are the Euler-LaGrange equations using the "space" LaGrangian

$$L = L(r, \dot{r}, \zeta, \dot{\zeta}, \theta) = \sqrt{r^2 + \dot{r}^2 + \dot{\zeta}^2} + \frac{e}{cp} \left[\dot{r} A_r + r A_\theta + \dot{\zeta} A_\zeta \right] \tag{3.3}$$

Consider the motion in the median plane ($z \equiv 0$) where the magnetic field has the form

$$B_z = -B_0\left(\frac{r}{r_0}\right)^k f(\theta);\ B_r = B_\theta = 0\ ;\ f\left(\theta + \frac{2\pi}{N}\right) = f(\theta) \tag{3.4}$$

In terms of the relative deviation from a circle of radius r_0, defined by

$$r = r_0(1+\chi) \tag{3.5}$$

the equation of motion following from (3.3) is

$$\frac{d}{d\theta}\left\{\frac{\dot{\chi}}{\sqrt{(1+\chi)^2+\dot{\chi}^2}}\right\} = \frac{1+\chi}{\sqrt{(1+\chi)^2+\dot{\chi}^2}} - \frac{e r_0 B_0}{cp}(1+\chi)^{k+1} f(\theta) \tag{3.6}$$

Three facts may be noted about (3.6). First, a particle of momentum p_1 satisfies the same equation about radius r_1 as a particle of momentum p about r_0 if $\frac{p_1}{p} = (r_1/r_0)^{k+1}$. It is thus clear that trajectories of particles of different energies differ from each other only by a scaling factor; the number of oscillations per revolution is therefore the same. Such an accelerator is called a "scaling" accelerator. Second, (3.6) has an inhomogeneous term

$$1 - \frac{e r_0 B_0}{cp} f(\theta)$$

and third, it has non-linear terms (arising both from kinematic effects and from the non-linear variation of field with radius). The non-linear terms are much more important than in conventional accelerators. Because of these non-linearities, the forced oscillation about the reference circle, caused by the inhomogeneous term, and the free oscillations about this forced solution do not superpose. The inhomogeneous term must be removed in order to calculate correctly the radial and vertical frequencies of oscillation.

To remove the inhomogeneous term, the equations of motion are written about an arbitrary curve $\underline{r}_e$ in the median plane. Thus

$$\underline{r} = \underline{r}_e + x\,\underline{n} + z\,\underline{b} \tag{3.7}$$

where

$$\begin{cases} \underline{r}_e' = \dfrac{d\underline{r}_e}{ds} = \underline{t} \;\; ; \;\; \underline{t}' = -\,\underline{n}/\rho \\ \underline{n}' = \;\; \underline{t}/\rho \;\; ; \;\; \underline{b}' = 0 \,, \end{cases} \tag{3.8}$$

where ds is the element of arc length along $\underline{r}_e$. The formulae (3.8) are the Serret-Frenet[4] formulae with the torsion $\frac{1}{\tau} = 0$. Denoting derivatives with respect to s by primes, it follows from (3.8) that

$$\underline{r}' = \left(1 + \frac{x}{\rho}\right)\underline{t} + x'\underline{n} + z'\underline{b} \,, \tag{3.9}$$

and by using this, the variational principle (3.1) may be written as

$$\delta \int_{s_1}^{s_2} \left\{ \sqrt{\left(1+\frac{x}{\rho}\right)^2 + x'^2 + z'^2} + \frac{e}{cp}\left[x'A_n + \left(1+\frac{x}{\rho}\right)A_t + z'A_b \right] \right\} ds = 0 \,. \tag{3.10}$$

The variational principle (3.10) is equivalent to a new "space" LaGrangian

$$\mathcal{L}(x, x', z, z'; s) = \sqrt{\left(1+\frac{x}{\rho}\right)^2 + x'^2 + z'^2} + \frac{e}{cp}\left[x'A_n + \left(1+\frac{x}{\rho}\right)A_t + z'A_b \right] . \tag{3.11}$$

The equations of motion which follow from (3.11) are

$$\frac{d}{ds}\left\{ \frac{x'}{\sqrt{\left(1+\frac{x}{\rho}\right)^2 + x'^2 + z'^2}} \right\} = \frac{1}{\rho}\frac{1+\frac{x}{\rho}}{\sqrt{\left(1+\frac{x}{\rho}\right)^2 + x'^2 + z'^2}} + \frac{e}{cp}\left[\left(1+\frac{x}{\rho}\right)B_b - z'B_t \right] \tag{3.12}$$

$$\frac{d}{ds}\left\{ \frac{z'}{\sqrt{\left(1+\frac{x}{\rho}\right)^2 + x'^2 + z'^2}} \right\} = \frac{e}{cp}\left[x'B_t - \left(1+\frac{x}{\rho}\right)B_n \right] .$$

The first of Eqs. (3.12) has an inhomogeneous term

$$\frac{1}{\rho} + \frac{e}{cp}B_b^e$$

where B_b^e is the vertical component of B along $\underline{r}_e$. This term vanishes when a particle of momentum p has the curvature $\frac{1}{\rho}$ in the field B_b^e, i.e., when its path $\underline{r}_e$ is a solution of (3.6). If further $\underline{r}_e$ is chosen to have the period of the magnetic field, the homogeneous differential equations will have only this period in s.

The curve $\underline{r}_e$ which has these properties is called the equilibrium orbit. It is a generalization of the equilibrium circle of conventional accelerators. Expanding (3.12) to first order in x and z gives the linearized equations of motion about such an equilibrium orbit

$$\begin{cases} x'' + \dfrac{1+n}{\rho^2}\, x = 0 \\ z'' - \dfrac{n}{\rho^2}\, z = 0, \end{cases} \tag{3.13}$$

where

$$n = +\frac{\rho}{B_b}\frac{\partial B_b}{\partial x} \tag{3.14}$$

is evaluated on the equilibrium orbit $\underline{r}_e$. In order to calculate n it may be noted that there is a unique relation between θ and s

$$s(\theta) = \int_0^\theta \sqrt{r_e^2 + \dot{r}_e^2}\, d\theta \tag{3.15}$$

and quantities along the orbit may therefore be discussed as functions of either s or θ. The variable

$$\vartheta = \frac{2\pi s}{s(2\pi)} \tag{3.16}$$

may also be used.

The magnetic field on the equilibrium orbit may be written using

$$F(s) = g(\theta) = \left(\frac{r_e}{r_0}\right)^k f(\theta) \,. \tag{3.17}$$

Then

$$B_b = \left(\frac{r}{r_e(\theta)}\right)^k g(\theta) = \left(\frac{r}{r_e(s)}\right)^k F(s) \tag{3.18}$$

and

$$\frac{\partial B_b}{\partial x} = \frac{\partial B_b}{\partial r}\frac{\partial r}{\partial x} + \frac{\partial B_b}{\partial \theta}\frac{\partial \theta}{\partial x} \,. \tag{3.19}$$

It is clear from Fig. 3 that

$$\begin{cases} \dfrac{\partial r}{\partial x} = \cos\phi \;;\; \dfrac{\partial \theta}{\partial x} = \dfrac{\sin\phi}{r_e} \\ \dfrac{dr_e}{d\theta} = -\, r_e \tan\phi \end{cases} \tag{3.20}$$

so that $$\left.\frac{\partial B_b}{\partial x}\right|_{r=r_e} = \frac{k g(\theta) \sec\phi + j \sin\phi}{r_e} .$$

Define ρ_o by $\rho_o = \rho F(s)$ and denote all quantities evaluated where $\rho = \rho_o$ with subscript o. Then

$$\frac{n}{\rho^2} = \frac{n_o}{\rho_o^2} F(s) \sec\phi \frac{r_o}{r_e(s)} + \frac{1}{\rho_o} \frac{dF}{ds} \tan\phi , \qquad (3.21)$$

where $n_o = \frac{k \rho_o}{r_o}$.

The Eqs. (3.13) may be written as

$$\begin{cases} x'' + \left[\frac{F^2(s)}{\rho_o^2} + \frac{n_o}{\rho_o^2} F(s) \sec\phi \frac{r_o}{r_e} + \frac{1}{\rho_o} \frac{dF}{ds} \tan\phi \right] x = 0 \\ z'' - \left[\frac{n_o}{\rho_o^2} F(s) \sec\phi \frac{r_o}{r_e} + \frac{1}{\rho_o} \frac{dF}{ds} \tan\phi \right] z = 0 \end{cases} \qquad (3.22)$$

The extra term in the radial equation comes, of course, from the centrifugal force and always aids focusing. The firstof the terms common to both equations is the usual gradient focusing. The radial (vertical) motion is focused (defocused) by the gradient in magnets of positive curvature and defocused (focused) in magnets of negative curvature. The second term gives "edge" focusing (also called "wedge" or Thomas focusing) and arises physically from the non-perpendicular entry into and exit from the field. This term is large when the field is changing rapidly along the equilibrium orbit and is defocusing for radial (x) motion and focusing for vertical (z) motion, since $F' \tan\phi < 0$ (except where a straight section is placed in the center of a negative magnet). In a radial sector FFAG accelerator with a small k the edge term is important for vertical stability, though the effect on the radialmotion is small. It is clearly necessary in the design of an FFAG accelerator to calculate the equilibrium orbit carefully, since the edge focusing terms are sensitive to its variation.

It is instructive to consider an ideal field which goes from its full value (F(s) = 1) to zero (F(s) = 0) in an arbitrarily short distance at s = 0. This is called the "hard edge" field. Then $F' = -\delta(s)$ and there is an instantaneous change of the slope or an orbit at the edge

$$\Delta(x') = \int_{\Delta s} \tan\phi(s)\,\delta(s)\,x(s)\,ds = \frac{x(0)\tan\phi(0)}{\rho_0}$$

$$\Delta(z') = -\frac{z(0)\tan\phi(0)}{\rho_0}$$

Consider the (2 x 2) matrix which transforms the (1 x 2) vector whose components are x and x' for the radial motion (and z and z' for the vertical motion). For the edge this matrix has the form:

$$\begin{pmatrix} 1 & 0 \\ \pm\tan\phi/\rho_0 & 1 \end{pmatrix} \tag{3.23}$$

where the positive (negative) sign is used for radial (vertical) motion. The hard edge theory is useful for preliminary calculations to investigate effects of some parameters such as k, magnet lengths and straight section lengths. It of course can give no information on effects of vertical gap size.

The Eqs. (3.22) have periodic coefficients and the form of their solutions is given by Floquet's Theorem.[5] The transformation matrix M for one period of either of the differential Eqs. (3.22) gives the phase change per sector σ by

$$\cos\sigma = \frac{1}{2}\,\mathrm{Trace}\{M\} \tag{3.24}$$

and the number of betatron wave lengths per revolution is $\nu = \frac{N\sigma}{2\pi}$

In radial sector machines the coefficients in (3.22) are even about the centers of magnets. If the transformation matrix from such a point of symmetry through a half sector is

$\begin{pmatrix} a & b \\ c & d \end{pmatrix}$

then by applying time reversal, the transformation matrix for the other half-sector is $\begin{pmatrix} d & b \\ c & a \end{pmatrix}$

and

$$\cos\sigma = ad + bc \quad . \tag{3.25}$$

Note that a and b are linearly independent solutions of (3.22) and c and d are their respective derivatives, all evaluated after one half period.

B. Design Calculations

During the design of this accelerator, magnetic field measurements had not been made, so that an experimental $f(\theta)$ was not available. The magnetostatic problem of finding $f(\theta)$ for given pole and current geometry is a very difficult one. The usual conformal mapping methods treat only two dimensional problems. However, in the present case, if effects of curvature and of k are neglected, so that the field is uniform radially, the problem reduces to the θ-ζ plane and conformal mapping methods may be applied. It was desired to have fields equal in magnitude on an equilibrium orbit within positive and negative magnets. To satisfy this condition, fields from two conformal problems were combined to give an approximate F(s) along an assumed equilibrium orbit, taken to be the hard edge orbit.[6] Each problem had only one of the two poles in a sector energized. The problem was done in this way to include the different path length of the orbit because it is not perpendicular to the magnet edges and to include the shift of the point of zero field between the magnets toward the positive magnet. This latter effect occurs because the field is stronger in the negative

magnet than in the positive magnet at a given radius by a factor $\left(r_e^+/r_e^-\right)^k$, where r_e^+ and r_e^- are the radii of the equilibrium orbit in positive and negative magnets. This shift is about 2 mm in this accelerator and has a small effect on particle motion. The two magnets were assumed infinitely thick and infinitely long in the conformal mapping, so that effects of other edges were neglected. Since the field was assumed uniform radially, the variation of potential along the pole faces due to the scalloping of the equilibrium orbit was neglected. The return currents of the pole face windings at the magnet edges were assumed of zero cross-sectional area, giving a discontinuity in potential.

The approximate F(s) found in this way can be used to find ϕ and r_e along the equilibrium orbit by using (3.18) and (3.20) to rewrite (3.6) as

$$\begin{cases} \phi' = \dfrac{F(s)}{\rho_0} - \dfrac{\cos\phi}{r_e} \\ r_e' = -\sin\phi \end{cases} \tag{3.26}$$

These equations cannot be solved in an unique way because F(s) must be recalculated for each new equilibrium orbit. In practice, with an approximate F(s), the results seem quite accurate in that F(s) does not change much when recalculated along the new orbit.

In the original design calculations, the above approximate method was used to find numerical values of ϕ and r_e. These values and power series approximations for F(s) gave power series solutions of (3.22) in various regions. In this way the elements of the transformation matrix were found numerically. The first effect investigated was the dependence of ν on vertical gap size. It was found that if the vertical gap is constant rather than proportional to the radius, then ν_z changes by about 20% across the

radial aperture, due to the different fringing effects at different radii. This is approximately equal to the spacing between integral and half integral resonances, so that it was considered necessary to scale the gap with radius, though this increases the current necessary in the pole-face backwindings. The dependence of frequencies on the form of F(s) in the fringing field was considered. The frequencies do not depend strongly on the shape of F(s), but are sensitive to the maximum value of ϕ attained along the equilibrium orbit, which depends essentially on the magnetic length of each magnet. Approximate forms for F(s) were used to determine parameters which would give the desired frequencies.

Because of the different dependences of ν_x and ν_z on gradient and edge focusing, it is possible to vary (or "tune") the two frequencies independently. Changing k changes ν_x more than ν_z and changing the "scalloping" of the equilibrium orbit by changing the relative currents in positive and negative magnets changes ν_z more than ν_x. These effects were calculated by using a new value of n_o in (3.22) in the first case and finding the new equilibrium orbit in the second case to give new values of ϕ and r_e in (3.22). The results of these calculations are

$$\frac{\Delta \nu_x}{\nu_x} \simeq \frac{1}{2} \frac{\Delta k}{k} \; ; \; \frac{\Delta \nu_z}{\nu_z} \simeq -\frac{1}{10} \frac{\Delta k}{k} \; .$$

$$\frac{\Delta \nu_x}{\nu_x} \simeq \frac{1}{3} \frac{\Delta B}{B} \; ; \; \frac{\Delta \nu_z}{\nu_z} \simeq \frac{3}{2} \frac{\Delta B}{B}$$

where Δ B is the difference in field intensity between positive and negative magnets.

C. Ex Post Facto Calculations

After the construction and operation of the accelerator, various calculations have been done to investigate orbit theory problems.

Using magnetic field measurements, (3.26) and (3.22) have been integrated numerically to find ν_x and ν_z. More extensive calculations have been carried out using the MURA IBM 704 high speed digital computer. The magnetostatic problem of the fields generated by the given iron and current distribution have been solved by use of a relaxation method proposed by L. J. Laslett[7] and programmed by J. N. Snyder (the Forocyl program). This method begins with the observation that in a scaling FFAG accelerator the three-dimensional Laplacian problem for the magnetostatic scalar potential Ψ may be reduced to a two dimensional problem. In the special case of a radial sector accelerator, the quantity

$$\Omega = \left(\frac{r}{r_0}\right)^{-(k+1)} \Psi \tag{3.27}$$

is a function only of the variables

$$\begin{cases} \xi = \dfrac{Ne}{2\pi} \\ \eta = \dfrac{Ns}{2\pi r} \end{cases} \tag{3.28}$$

and satisfies the equation

$$\frac{\partial^2\Omega}{\partial\xi^2} + \left(1 + \frac{4\pi^2\eta^2}{N^2}\right)\frac{\partial^2\Omega}{\partial\eta^2} - \frac{4\pi^2(2k+1)}{N^2}\eta\frac{\partial\Omega}{\partial\eta} + \frac{4\pi^2(k+1)^2}{N^2}\Omega = 0 . \tag{3.29}$$

Ω is an odd function of η and is periodic in ξ with period one. Prescribed boundary values are entered on a two-dimensional grid and will be satisfied by the solution, which is given in the form of numerical values at points on this grid. These boundary values represent iron surfaces of infinite permeability. Effects of currents are taken into account by discontinuous jumps in Ω at grid points where currents are placed.

The Forocyl program can also be used to integrate the simpler equation

$$\frac{\partial^2\Omega}{\partial\xi^2} + \frac{\partial^2\Omega}{\partial\eta^2} = 0 \tag{3.30}$$

with the same boundary conditions. This equation neglects effects of finite k and effects of the third (radial) dimension, which exist even when k = 0. However, it may be seen that with k = 0 only the η^3 term of Ω is affected by the difference between (3.29) and (3.30). The median plane fields ($\frac{\partial \Omega}{\partial \eta}\Big|_{\eta=0} = -B_b$) and their first derivatives, ($\frac{\partial B_b}{\partial x}$) , as determined from (3.29) or (3.30), differ only by finite k effects. The frequencies of oscillations are determined by these quantities in the linear approximation.

The original design calculations correspond exactly to the approximations used in (3.30) except that each of the poles in the conformal mapping method of the design was assumed semi-infinite azimuthally and vertically; also, the variation of potential along the pole faces due to scalloping of the equilibrium orbit has been included in the calculations done with (3.30), but not in the design calculations. The more exact calculations done with (3.29) correspond to the actual magnets except for finite permeability effects.

The magnetic fields generated by the Forocyl program are stored on a two dimensional mesh and used in the solution of the dynamical equations derived from the LaGrangian (3.3) in the Formesh program of the MURA Computer. This program is due also to L. J. Laslett and J. N. Snyder.

Two separate calculations have been done with the Forocyl and Formesh programs. Both calculate ν_x and ν_z with the magnets and currents of the present accelerator. Calculation 1 used (3.29) to generate the fields from the poles, while calculation 2 used the simpler and less accurate (3.30). Results of both calculations are given in Sec. IX .

IV. MAGNETS

The general structure of the magnets is illustrated in Figs. 4 and 5. The magnets have plane pole faces machined from forged slabs of SAE #1005 low carbon steel 1-1/8 in. thick. The pole face coils are wound with number 22 formvar insulated wire. Support for the coils is provided by a 0.025 in. dural plate in the shape of the pole face. Coil forms were machined from lucite with grooves for holding the wire 0.0005 in. less in width than the diameter of the wire. If the iron surfaces were equally spaced along equilibrium orbits, the pole face windings would parallel the equilibrium orbit. However, since the pole faces are flat and the gap increases with radius, it may be shown that, in the first approximation, these windings follow arcs of radius $\frac{k+1}{k}\rho$ to terminate properly the magnetic potential at the surface of the iron, neglecting fringing effects. The coils were wound on the forms and the supporting plates were attached to the wires with an epoxy resin cement (Araldite 104 or Hysol 2060) which adheres to formvar and aluminum but not to lucite. After the cement hardened, the coils could be stripped from the forms. Due to progressively closer spacing of the wires with increasing machine radius, it was necessary to have two layers of windings over the outer half of the coils. The second layer was cemented to the opposite side of the supporting plate. Water cooling pipes run through the thick portions of the coil bundle.

Field and field gradient measurements were made with a flip coil and fluxmeter. The flip coil assembly is mounted on a frame which permits radial and azimuthal positioning of the coil. Measurements of the field were made in the median plane at a number of points along the centers of the magnets and azimuthally at three

different radii. Three coils are mounted on the shaft with the central coil used for field magnitude measurements and the three coils connected as in Fig. 6 for field gradient measurements. Coils 1 and 3 are connected in series bucking so that when the fluxmeter indicates a null, the potentiometer reading is proportional to $\frac{B_3 - B_1}{B_2} = \frac{\Delta B}{B}$; therefore k can be obtained directly from the potentiometer reading. This bridge method makes it possible to measure k to a relative accuracy of the order of 0.1%.

It was observed that in the low field regions the results of measurements made on an isolated magnet were different from those made on the same magnet when it was flanked by other magnets. This was true even along the central line of the magnet where fringing is negligible. This effect is presumed to be due to the variation of permeability of the iron in the magnet return yoke with flux density. For this reason, the field measurements were made with guard magnets on either side of the one being measured to simulate actual operating conditions.

In order to reproduce fields it was found necessary to return the current to zero whenever any changes in current were made. This current cycling was always done by switching off and on the primary power of the magnets; reducing the currents slowly to zero and raising them slowly gave different resulting fields from the switching process. This strong dependence on magnetic history was very evident in subsequent studies with the electron beam.

The field gradient was adjusted by changing the number of turns around the return yoke until k and B at the injection radius were within $\pm$ 1% of the mean values. Since this was the only correction applied to the calculated current distributions, it appears that at least along magnet centers the iron may be considered to have zero

reluctance. The reinforcing currents on the return yokes of the magnets apparently compensate for the finite reluctance of the return yokes. Except for a slight deviation at the point where the second layer of the pole face coil begins, k remains constant to within ± 1% along the central line of each magnet. The field gradient can be changed for tuning purposes by running current through a separate twenty turn return yoke winding. This change of k does not scale, being greater at small radii than at larger ones.

The magnet coils in the assembled accelerator are connected with the positive magnets in one series circuit and the negative magnets in a separate series circuit. This enables one to tune by changing the relative currents in the positive and negative magnets. Power for the magnets is supplied by a selenium rectifier power supply. Although it would be a convenience, it has not been necessary to stabilize or regulate this supply to maintain steady and reproducable beams under favorable tuning conditions.

V. ACCELERATOR CONSTRUCTION

The overall structure of the accelerator is seen in Fig. 7, and a detail of a portion of the accelerator with one magnet removed appears in Fig. 8. The accelerator is built on a 1-1/4 in. cast aluminum plate supported at three points by aluminum legs. This table is cut at two azimuths and cemented to an insulating sheet with thermo-setting plastic to avoid short circuiting the betatron accelerating core. Holes were precision jig-bored through the table and dowel pins, inserted from below through those holes into matching holes in the magnets, position all magnets to within 0.001 in. The table is flat to within 0.003 in. The vacuum tank is made of welded aluminum, and is in two halves, bolted together with teflon gaskets again to avoid short circuiting the betatron.

The tank is evacuated with a four-inch oil diffusion pump backed by a booster oil diffusion pump and a mechanical pump. A refrigerated baffle is used and a vacuum between 10^{-5} mm and 10^{-6} mm of Hg is standard in this system. Access ports around the inside of the tank are provided at the centers of magnets except for regions obstructed by the pump-out manifold. There are also ports on the outside circumference of the tank between every pair of magnets except at the points where the two halves of the tank are joined.

Injection is by means of an electron gun of the type used in the University of Illinois 80 Mev betatron. It may be used as a pulsed or continuous source of electrons. For pulsed operation a delay line is discharged through the primary of a pulse transformer to provide pulses of from a few tenths of a microsecond to three microseconds in duration. Operating from a D.C. high voltage supply three milliamperes of continuous beam may be injected.

The betatron core is excited sinusoidally by a 500 cycle generator to provide approximately 40 volts per turn maximum to the electrons. The 500 pounds of 0.014 in. transformer iron in the core are driven to $\pm$10,000 gauss dissipating 6 kilowatts of heat at full excitation, and water cooling of the laminations is provided. An alternate pulsed supply employing FG 105 thyratrons has also been employed permitting more flexible acceleration programming.

Without some additional mechanism to expand the equillibrium orbit away from the injector rapidly during the first few turns around the machine the beam might be lost due to striking the injector anode, which protrudes radially about two mm beyond the filament; the 40 volts from the betatron core increases the orbit radius only 0.08 mm per revolution at injection. The expander mechanism which is used consists of the circuit shown in Fig. 9a.

The 0.05 μf condenser is discharged through the one microhenry inductance of the vacuum tank of the accelerator by means of a 5C22 hydrogen thyratron. Since the thyratron will not conduct in the backward direction, this results in a voltage wave form across the accelerating gap which is approximately one half of a cosine curve having the resonant frequency of the 0.05 μf condenser and tank inductance combination, (Fig. 9b). Injection takes place during the second (positive) portion of the waveform and the electrons receive about 500 volts per turn at the peak voltage. Longer expansion pulses for use with longer injection pulses are provided with the same circuit driving a 2 to 5 turn coil placed around the machine.

VI. STATIC MEASUREMENTS OF BETATRON FREQUENCIES

The first tests of betatron oscillation wave lengths were made using a special injector which produces a continuous beam of electrons through a one millimeter hole in its anode. This injector was placed at the center of a positive curvature magnet; at the center of the next positive magnet a metal plate with several small equally spaced holes was placed to define rays of electrons. These rays then produced bright spots on a zinc sulphide fluorescent screen placed at the center of a subsequent positive magnet. These spots could be observed visually through a lucite port in the vacuum tank and their separations determined using a one millimeter grid ruled onto the screen. From Floquet's Theorem[5] for linear oscillations, σ_x can be determined from the ratio of the separation of two radial images on the screen m sectors beyond the injector, Δx_m, to the radial separation of two holes in the metal plate, Δx_1, when the injector, plate, and screen are at homologous points in the magnet structure:

$$\frac{\Delta x_m}{\Delta x_1} = \frac{\sin m\sigma_x}{\sin \sigma_x} \qquad (6.1)$$

A similar expression holds for σ_z.

With m = 2, values of σ_x and σ_z were found in the above manner for several tuning conditions. However, due to non-linear effects, (6.1) is only approximate. More accurate determinations of σ's were made with the screen placed seven sectors beyond the injector. In this case, the machine was tuned (by varying the ratio of magnet currents) until a small group of rays came to a focus. In radial sector accelerators with non-linearities present, a group of rays can come to a focus only at the maxima of the oscillations of the central ray of the group. When such a focus is obtained, the path length between the injector and screen is an integral or half integral number of betatron oscillations of the central ray about the equilibrium orbit. If the tuning conditions for two successive nodes are know, σ for other tunings may be found by interpolation. Vertically, the current ratio tuning range is large and two nodes were obtained; interpolation between the nodal tunings agreed with a modification of (6.1) applied to the spacing of one pair of rays of quite different amplitudes. Since only one node was obtained radially (due to the smaller range of radial tuning) this modification of the two ray method was used to find σ_x. The results for small amplitude are given in Section IX.

It was possible by the above method to study the variation of σ_x with amplitude. The x amplitude was changed by moving the equilibrium orbit relative to the injector (changing the injection voltage). The tuning was then changed until a group of rays was brought to a focus (corresponding to an odd half integral number

of oscillations). The oscillation amplitude then is half the difference between the injector radius and the radius of the focused rays on the screen. With these data on the tuning change with amplitude for a given frequency, and the frequency change with tuning from the previous measurements, the results indicate σ_x is reduced by several per cent at 2 cm amplitude of oscillation from its value at zero amplitude. Since σ_x is close to the major resonance, $2\pi/3$, accurate quantitative interpretation of this data in terms of σ_x versus amplitude is not reliable; however, the sign and magnitude of the effect agree with subsequent digital computer results.

VII. ACCELERATED BEAM

A. Pulsed Injection

With the standard pulsed injector, the accelerator is generally operated using the expander and injection pulses of a fraction of a microsecond in length. Accelerated beam may be detected either by observing x-rays from a target probe or by charge collection on the target probe. The electron energy may be deduced from the time delay of the beam pulse from injection, from the radial position of the probe, the electron revolution frequency (Sec. VIII), and from the x-ray energies. With 40 volts energy gain per turn, the beam reaches full energy in 160 microseconds. With pulsed core excitation, beam may be accelerated to an intermediate energy in the machine, allowed to coast there for up to five milliseconds, and then betatron accelerated to the target. It is of interest to note that the electrons detected after five milliseconds have traversed about 3×10^6 non-linear sectors. Such a coasting beam is attenuated considerably by gas scattering; measurements have been made on the half life of the beam by varying the turn on time for the second acceleration pulse. For

example, at a pressure of 2.5×10^{-6} mm Hq and a vertical aperture of about one cm the beam half life at about 300 kilovolts is 600 microseconds. From charge collection, the beam is found to contain of the order of 10^8 electrons per pulse, no correction being made for scattering or secondary emission from the target.

Under certain tuning conditions, considerable beam is captured and accelerated without the expander. It is observed that the beam intensity in this case is virtually unchanged by increasing the injector pulse length from a fraction of a microsecond to three microseconds, possibly indicating that the mechanism for missing the injector is related to transient space change effects.

Although beam is obtained under a variety of tuning conditions, as will be discussed later, the most reliable operating region, and consequently the usual operating conditions correspond to ν_x of about 2.75 and ν_z of about 1.75.

B. Continuous Injection

Although the major purpose of this model is to study FFAG problems pertaining to the design of very high energy accelerators, a promising application of FFAG is in high intensity electron betatrons of medium energy using continuous injection. Since the guide fields are time independent, electrons of all energies are accelerated as long as the betatron flux continues to rise. To examine this possibility, the injector of the model was connected to a D.C. power supply and operated at about three milliamperes continuous emission. Accelerated beam was found over a full 600 microseconds, repeating every two milliseconds (the betatron flux period with sinusoidal excitation.) Tuning conditions to obtain beam were somewhat more critical than with pulsed injection using the expander. With

optimum tuning the electrons collected on the target prove gave a time average current of at least 1.5×10^{-8} amperes, or about 10^8 electrons per pulse. Under these conditions the capture efficiency from the conventional betatron gun was quite low. From simple orbit theory it is not apparent in this case how electrons miss striking the back of the injector in the absence of transient space charge effects. One possibility is that a field perturbation with a strong radial dependence, such as electrostatic fields from the injector, could enable particle orbits to move away from the injector more rapidly than the average spiralling due to betatron acceleration. In order to realize fully the high intensity potentialities of continuous injection, injector systems designed specifically for the purpose must be developed.

VIII. RADIO FREQUENCY EXCITATION OF BETATRON OSCILLATIONS

In addition to the static one turn method of determining frequencies of betatron oscillation, discussed in Section VI, a dynamic method using the accelerated beam is also employed. This technique, previously used on the University of Michigan synchrotron,[8] consists of applying an rf electric field perpendicular to the particle orbit and observing the frequencies of this rf which drive the betatron oscillations in resonance.

A. Calculation of Rf Resonance Frequencies

The rf frequencies which may perturb the beam can be easily found. Assume the rf field is uniform and a delta function of azimuth. Then the equation representing the x oscillations of a particle is approximately

$$\frac{d^2x}{d\vartheta^2} + \nu_x^2 x \cong A\, e^{i\frac{f_{rf}}{f_0}\vartheta} \sum_m e^{im\vartheta}, \qquad (8.1)$$

where m is an integer, f_{rf} is the rf oscillator frequency, and f_o is the particle revolution frequency; ϑ , the independent variable, defined in Eq. (3.16), equals $2\pi f_o t$.

The x oscillation grows when

$$f_{rf} = | \nu_x \pm m | f_o \, . \tag{8.2}$$

An integral number of extra betatron or rf oscillations per revolution clearly makes no difference in the phase of the force on the particle as it passes the rf kicker.

If there are spatial gradients in the rf field, the relation for resonance is

$$f_{rf} = | p\nu_x + q\nu_y \pm m | f_o \, , \tag{8.3}$$

where p and q are positive integers and $1 \leq p+q \leq 4$.[9,10] It is also possible for the amplitude of oscillation to grow when p or q is greater than one and the rf field is uniform, if there are non-linearities present in the particle equation of motion; any such effects here would be masked by the electric field gradients.

B. Experimental methods

To excite betatron oscillations in the model, rf is applied to a pair of small brass plates placed above and below the beam at the radius of the target probe. The rf oscillator, tied to the plates, is tunable from 5 to 60 Mc and delivers up to 300 volts. The electron frequency of revolution goes from about 35 Mc at injection to 75 Mc at maximum energy. Throughout the measurements $f_{rf} < f_o$.

Both radial and vertical betatron oscillations can be excited by the rf on the plates, the electrons apparently seeing both radial and vertical components of electric field. A difference in beam behavior usually makes it possible to determine which oscillation is being

excited; when radial oscillations are driven, the beam is observed to strike the target earlier in time; when the vertical oscillations are excited, however, the beam strikes the vacuum tank and is not observed on the target probe.

The rf frequencies which perturb the beam occur in pairs; that is, if $f_{rf_1} = (\nu_x - m) f_o$ is a resonance, then so is $f_{rf_2} = (m+1-\nu_x) f_o$. The sum of these two measured frequencies must add up to f_o, the revolution frequency. If ν_x is known to within a half integer by other methods, its value is then determined. Rf frequencies are found not only for ν_x and ν_z, but also for 2 ν_x, 2 ν_z, and $\nu_x + \nu_z$, as expected with gradients in the rf field. A typical set of frequency measurements, assignments and results is given in Table II.

TABLE II. Determination of ν_x and ν_z from rf resonance frequencies

Measured frequency f_{rf}	Type of oscillation	fo Mc	f_{rf}/fo	Assignments[a] f_{rf}/fo	Results[b]
16.5	ν_z		.223	$2 - \nu_z$	
57.5	ν_z	74	.778	$\nu_z - 1$	$\nu_z = 1.78$
23	x		.311	$3 - \nu_x$	
51	x	74	.690	$\nu_x - 2$	$\nu_x = 2.69$
35	z (?)		.466	$(\nu_x + \nu_z) - 4$	
40	?	75	.533	$5 - (\nu_x + \nu_z)$	$\nu_x + \nu_z = 4.47$
27	x		.365	$2\nu_x - 5$	$2\nu_x = 5.37$
30	x		.406	?	

a. Sum of the two f_{rf}.

b. Other methods indicate that for these tuning conditions $2.5 < \nu_x < 3$ and $1.5 < \nu_z < 2$.

The values of ν obtained in this way appear reproducible and reliable to better than one percent. No appreciable changes in the

ν's have been observed when the vertical aperture was limited or when misalignments generated deviations of the equilibrium orbit. Tests near the injector indicated that the radial betatron oscillations are probably less than 1 cm so the frequencies measured should be those for small amplitude oscillations.

SEC. IX. THEORETICAL AND EXPERIMENTAL VALUES OF BETATRON FREQUENCIES

Measured and calculated values of ν_x and ν_z for the design conditions (no k correction, current ratio unity) are given in Table III.

TABLE III. Comparison of measured and calculated betatron oscillation frequencies

	Dynamic measurements	Static measurements	Design calculations	Calculation 1 with Computed fields	Calculation 2 with Computed fields	Calculation with measured fields
ν_x	2.85 ± 0.02	2.87 ± 0.06	2.80	2.83	2.78	2.84 ± 0.05
ν_z	2.18 ± 0.02	2.12 ± 0.06	1.80	2.02	1.86	2.13 ± 0.10

The dynamic measurements, obtained by methods described in Sec. VIII, and the static measurements, Sec. VI, are in agreement with one another. The dynamic measurements are most precise and should be used in comparisons with theory. The dynamic measurements have been done at various radii and within the limits of experimental error the ν's are independent of radius, confirming the scaling nature of the fields.

The methods used in the design calculations are described in Part B of Sec. III and the other later calculations in Part C of Sec. III. Calculation 1 is done using the Forocyl program with effects of finite k included, while calculation 2 uses the same program with these effects neglected.

Calculation 1 neglects only the finite permeability of the real magnets and should be compared with the measured ν's. The two values of ν_x are seen to be in excellent agreement. The 7% error in ν_z may be partly due to finite permeability effects. It should also be noted that misalignments or finite amplitudes of oscillation, which are present in the machine but not in calculation 1, may change the ν's because of non-linear terms in the equations of motion; these effects, which are discussed in Sec. VIII, are believed to be small for the accelerated beam.

Calculation 2 makes essentially the same approximations as the design calculation and should be compared with it. The ν_x's are again in excellent agreement. The 3% difference in ν_z between the two is believed to be due mostly to the variations of poleface potentials included in calculation 2, but not in the design. Other numerical calculations have shown this effect to be of this magnitude and sign. Thus the large (approximately 18%) difference between the design and measured values of ν_z appears to be due partly to k effects (8%) and scalloping effects (3%) neglected in the design, while the remainder is due to effects such as finite permeability, misalignments and non-linearities.

The calculation with measured fields and the experiments agree within the ascribed errors. The errors given for the calculation are due to positioning uncertainties (about 0.1°) of the flip coil used in the field measurements. Measurements were made between the centers of two adjacent magnets. An error in the position of a center point can cause relatively large amounts to be added to or subtracted from the magnetic length of each sector, changing the scalloping of the equilibrium orbit and ν_z.

It is of interest to note here the relative insensitivity of ν_x to the approximations of the different calculations, and conversely the sensitivity of ν_z. This sensitivity of ν_z is particularly pronounced in machines with large flutters and large equilibrium orbit scalloping, such as the present one. It is of course because of this sensitivity of ν_z to flutter that such a broad range of ν_z may be easily covered by current ratio tuning.

X. PERTURBATIONS

Experiments and calculations have been performed to test the effects of machine imperfections or misalignments on the equilibrium orbits by displacing entire magnets.

A. Calculation

With misalignments, as in the present calculation, the period of the structure and hence the period of the equilibrium orbit is one revolution, rather than one sector. The displacement of the equilibrium orbit from its unperturbed form is calculated below in the linear approximation.

Since an entire magnet is moved in the experiments, the motion of a particle inside a displaced magnet is unchanged by the perturbation. Therefore, the matrix which transforms the particle displacement y and its derivative y' through the magnet which is displaced an amount Δy is unchanged. However, y in the unperturbed machine is replaced by $y - \Delta y$ at both boundaries of the displaced magnet, while y' is unchanged at the boundaries. By transforming with matrices through the undisplaced remainder of a revolution the new equilibrium orbit may then be found. This method neglects changes in the fringing field, which do not enter in the approximation used below. It should be noted also that in the radial experiments, the magnet dis-

placement and orbit displacement are measured radially from the center of the machine and not perpendicular to the equilibrium orbit, which is "scalloped" even without misalignments. Since the orbit displacement is proportional to the magnet displacement in the linear approximation, the error cancels.

The two magnets of a sector are denoted by the subscripts "a" and "b". Transformation matrices are used between the centers of straight sections. The transformation matrix for one sector

$$M_1 = M_b M_a \tag{10.1}$$

has the form[11]

$$M_1 = M(\sigma, \alpha, \beta) = \begin{pmatrix} \cos\sigma + \alpha \sin\sigma & \beta \sin\sigma \\ -\frac{1+\alpha^2}{\beta} \sin\sigma & \cos\sigma - \alpha \sin\sigma \end{pmatrix} \tag{10.2}$$

and

$$M_m = (M_1)^m = M(m\sigma, \alpha, \beta). \tag{10.3}$$

It is convenient to define the vector

$$Y_i = \begin{pmatrix} y_i \\ y_i' \end{pmatrix} \tag{10.4}$$

and choose i = 0 at the center of the straight section immediately after the bumped magnet. Consider b to be the displaced magnet. Then

$$Y_r = M_r Y_0 = M_a M_{N-1} Y_0 \tag{10.5}$$

is the displacement vector at the center of the straight section immediately preceding the bumped magnet. The equilibrium orbit is then the solution of the equations which follow from (10.5) and

$$\begin{pmatrix} y_0 - \Delta y \\ y_0' \end{pmatrix} = M_b \begin{pmatrix} y_r - \Delta y \\ y_r' \end{pmatrix}. \tag{10.6}$$

Defining the matrix elements by

$$M_i = \begin{pmatrix} a_i & b_i \\ c_i & d_i \end{pmatrix} \quad \text{with} \quad a_i d_i - b_i c_i = 1, \tag{10.7}$$

the combination of (10.5) and (10.6) gives the set of linear inhomogeneous equations

$$\begin{cases} (a_N - 1)\, y_0 + b_N\, y_0' = (a_b - 1)\, \Delta y \\ c_N\, y_0 + (d_N - 1)\, y_0' = c_b\, \Delta y \end{cases} \tag{10.8}$$

Using $a_N + d_N = 2\cos N\sigma$, the solution of (10.8) is

$$\begin{cases} y_0 = \dfrac{\Delta y}{2(1 - \cos N\sigma)} (1 + d_r - a_b - d_N) \\ y_0' = \dfrac{\Delta y}{2(1 - \cos N\sigma)} (c_N - c_b - c_r) \end{cases} \tag{10.9}$$

Displacements at homologous points around the machine may be found by applying the transformation matrix M_1 to Y_0.

To find values for the matrix elements in (10.9) the "hard-edge" approximation was used with an orbit geometry which gave $\nu_x = 2.71$, $\nu_z = 1.73$, values close to those for which the experiments were performed, $\nu_x = 2.69$, $\nu_z = 1.77$.

By Floquet's Theorem,[5] the displacements at homologous points lie on a sine curve of frequency ν and amplitude $A = \sqrt{y_m^2 + (\alpha y_m + \beta y_m')^2}$ which is invariant (independent of m). Calculated values of this invariant are given in Table IV.

TABLE IV Maximum displacement of the equilibrium orbit with a magnet misalignment calculated at the centers of straight sections

	$A/\Delta y$
Wide magnet moved radially	1.6534
Narrow magnet moved radially	0.3013
Wide magnet moved vertically	0.8089
Narrow magnet moved vertically	1.9423

These sine curves are used in the graphical comparison of theory and experiment below.

B. Experimental Procedure

Two experiments were carried out; one for radial misalignments and one for vertical misalignments. For the vertical bumps, a probe was used consisting of a wire mounted parallel to but about 1 cm off the axis of a shaft which extended radially into the tank at the center of a straight section. The probe could be moved radially to detect the beam at different energies and by rotating it the vertical position of the beam could be found. This was done by observing the x-ray yield versus angular rotation of the probe. The scintillation detector is placed either near it or near a fixed broad target at a different azimuth and at a radius slightly greater than that of the probe tip. The vertical position of the probe where all beam strikes it corresponds to the equilibrium orbit at that azimuth. To determine the effect of one displaced magnet on the equilibrium orbit around the machine, the inverse experiment was done, finding the change in position of the equilibrium orbit at the probe azimuth while displacing each magnet vertically in turn around the machine. Displacements were 0.045 in. produced by shimming. The experimental results are plotted in Fig. 10 with the theoretical curves.

Radially, measurements were made by determining the radial separation between the probe and the fixed target (located in diametrically opposite straight sections) when the beam was divided almost equally between the two. This radial separation was found for a given radial displacement (0.062 in.) of each magnet in turn around the machine. The results are also given in Fig. 10. These are compared with differences between calculated values in diametrically opposite straight sections.

The error on experimental points vertically is due chiefly to determination of the probe angle. The readings were taken to the nearest 5^{o}, corresponding to an estimated error of about 0.4 in units

of the vertical bump. All points agree with calculatons to better than 0.8 except one large error (y_3 for wide magnets).

Radially, the experimental points are averages over data from outward and inward displacements. Occasionally the data were different, presumably due to non-linearities causing different phase shifts. The overall accuracy of the radial points is estimated to be $\pm$ 1/64 of an inch, corresponding to $\pm$ 0.25 in units of radial displacement. All radial points agree with calculations to an accuracy of 0.5 or better.

The graphs indicate good agreement between the hard edge theory and the experimental results.

XI. RESONANCE SURVEY

The intensity of accelerated beam has been measured over a large section of the ν_x - ν_z stability region in this accelerator in order to study the effects of various resonances.[12]

A. Method

The working point of the machine was varied by changing k and the magnet currents, as discussed earlier in Sec. III and IV. Since any changes in k do not quite scale the survey measurements were made fairly close to the injector.

A region of the ν_x - ν_z plane was covered corresponding to ν_z of from 1 to 3 and to ν_x of from 2.3 to 3. Measurements of the betatron oscillation frequencies were made using the rf resonance technique on the accelerated beam (Section VII). Intensity of the beam was indicated by pulse height on a scintillation detector. The frequencies were most conveniently changed by holding k constant and varying the current ratio and vice-versa. Intensities and measured

frequencies from one current ratio tuning run are shown in Fig. 11. Indicated are the possible positions of resonances, found by interpolation between points of measured frequency. A similar plot for a k tuning run is shown in Fig. 12. As indicated on the figures, a current ratio tuning run changes ν_z almost exclusively while a k run changes only ν_x, in agreement with part B of Section III.

All of the data for this survey were taken with pulsed injection, using the expander and the same magnet configuration. Due to differences in peak energy, beam length, and beam shape corresponding to different tuning positions, the photomultiplier pulse height is not exactly proportional to the number of electrons. However these corrections should be small relative to the range of intensities studied.

B. Results

The data from a number of tuning runs have been used to construct a contour map of beam intensity of a $\nu_x - \nu_z$ diagram, Fig. 13. The contours indicate constant beam intensity, successive contours differing by $\sqrt{10}$ in intensity. Outside the last contour, the beam intensity is not measurable. Table V presents the decrease in beam intensity in the regions of particular resonance lines, along with the stop band widths where the beam is completely destroyed. Also indicated are the number of places each resonance was crossed in the tuning runs and the number of places a decrease in intensity was observed.

TABLE V. Results of resonance survey

Resonance	Number of[a] Places Crossed	Number of Places Seen	Percentage Decrease in Intensity	Stopband Width
Integral				
$\nu_z = 1.0$		2[b]	100	+0.08
$\nu_z = 2.0$	5	5	100	±0.12
$\nu_z = 3.0$		1[b]	100	-0.10
$\nu_x = 3.0$		4[b]	100	- .12
Half Integral				
$2\nu_z = 3$	4	4	100	±0.01
$2\nu_z = 5$	4	4	100	+0.02
$2\nu_x = 5$	2	2	100	±0.02
$\nu_x + \nu_z = 4$	4	4	100	+0.01
$\nu_x + \nu_z = 5$	3	3	100	±0.01
$\nu_x - \nu_z = 0$	2	0		
$\nu_x - \nu_z = 1$	4	0		
Third Integral				
$3\nu_z = 4$	4	0		
$3\nu_z = 5$	5	2[c]	33[c]	
$3\nu_z = 7$	3	1[d]	70[d]	
$3\nu_z = 8$	1	0		
$3\nu_x = 7$	1	0		
$3\nu_x = 8$	3	3	100	±0.01
$\nu_x + 2\nu_z = 5$	3	3	85	
$\nu_x + 2\nu_z = 6$	3	3	80	
$\nu_x + 2\nu_z = 7$	2	0		
$\nu_x + 2\nu_z = 8$	2	2	100	±0.01
$2\nu_x + \nu_z = 6$	2	0		
$2\nu_x + \nu_z = 7$	2	0		
$2\nu_x + \nu_z = 8$	3	3	75	
$2\nu_z - \nu_x = 0$	4	0		
$2\nu_z - \nu_x = 1$	2	0		
$2\nu_x - \nu_z = 3,4$	≥1	0		
Fourth Integral				
$4\nu_z = 5,7,9,11$	≥1	0		
$4\nu_x = 11$	2	0		
$\nu_x + 3\nu_z = 6,7,8,11$	≥1	0		
$3\nu_x + \nu_z = 9,10,11$	≥1	0		
$2\nu_x - 2\nu_z = 0,2$	≥2	0		
$3\nu_z - \nu_x = 4$	1	0		

a. When not obscured by a stronger resonance
b. At tuning limit
c. Uncertain
d. Undoubtedly due to $2\nu_x + \nu_z = 8$.

C. Discussion

Eq. (3.12) can be expanded in powers of x and z to give the approximate equations of motion for the accelerator, considered as a perfect machine

$$\begin{cases} \frac{d^2x}{d\theta^2} + \nu_x^2 x = b_x(\theta)x^2 + c_x(\theta)z^2 + d_x(\theta)x^3 + e_x(\theta)xz^2 \\ \frac{d^2z}{d\theta^2} + \nu_z^2 z = b_z(\theta)xz + d_z(\theta)z^3 + e_z(\theta)x^2z \end{cases} \qquad (11.1)$$

where the linear coefficient has been replaced by an equivalent frequency and the coefficients of the non-linear terms are periodic with period $2\pi/N$ in the azimuthal variable.

Part of the character of the non-linear terms is due to symmetry of the magnetic fields about the median plane: only terms of even power in z appear in the radial equation of motion and only terms of odd power in z appear in the vertical equation. Imperfections will add other terms to the right hand sides of the equations, such as $u(\theta)x^p z^q$, $u(\theta)$ being periodic with period 2π, its magnitude and Fourier components dependent on the imperfections.

Moser[9] and Sturrock[10] have shown that when the radial equation contains a term of the form

$$\cos m\theta \; x^{p-1} z^q$$

where m, $p \geq 1$ and $q \geq 0$ are integers, then there are resonant phenomena when

$$p\nu_x + q\nu_z = m \qquad (11.2)$$

This relation results also from a term in the vertical equation of the form

$$\cos m\theta \; x^p z^{q-1}$$

where m, $p \geq 0$ and $q \geq 1$ are again integers. There are stable oscillations up to some finite amplitude when $p + q > 4$ and in some

cases when $p + q = 4$. The relation

$$p\nu_x - q\nu_z = m$$

does not lead to instability.

The integer m in (11.2) labels the Fourier component of the coefficient of the non-linear term which drives the resonance. A case of great importance is m = 8, the number of sectors in this machine. Here the periodic non-linear terms give rise to instabilities even without any imperfections. These are sometimes called inherent or sector resonances as opposed to the usual imperfection or machine resonances.

Integral Resonances $p + q = 1$

These resonances, driven by imperfection forcing terms independent of oscillation amplitudes, completely destroy the beam over a large stop band $\Delta\nu = \pm 0.1$. As seen in Section X on misalignments, a displacement of one magnet produces a comparable displacement of the equilibrium orbit, even between resonances. The equilibrium orbit undergoes large oscillations near resonance, so that a large stop band is easy to understand. It is possible that part of the stop band about $\nu = 3$ is due to difficulty in missing the injector.

Half Integral Resonances $p + q = 2$

Such resonances are driven by imperfection terms linear in the oscillation amplitudes. The difference resonances do not affect the beam, but the other resonances destroy it with a stop band width of $\Delta\nu = \pm 0.01$, a band much smaller than that caused by the integral resonances. These integral and half integral stop band widths are comparable to those observed in the Brookhaven analogue.[12]

Third Integral Resonances $p + q = 3$

Terms quadratic in oscillation amplitudes drive these resonances.

As seen from Eqs. (11.1) such terms would be present in this accelerator even without any imperfections. The inherent resonances arising from these terms are

$$3\nu_x = 8$$
$$\nu_x + 2\nu_z = 8.$$

Both of these resonances completely destroy the beam, with a stop band width of $\Delta\nu = \pm 0.01$. The third integral imperfection resonances often affect the beam, but never completely destroy it. The imperfection resonances which attenuate the beam are

$$\nu_x + 2\nu_z = m$$
$$2\nu_x + \nu_z = 8.$$

Again, no difference resonances are observed including $2\nu_z - \nu_x = 0$.[13]

Fourth Integral Resonances $\quad p + q = 4$

Terms cubic in the oscillation amplitudes drive these resonances. Inherent resonances, from terms in Eqs. (11.1) are

$$4\nu_z = 8$$
$$2\nu_x + 2\nu_z = 8.$$

These resonances conincide with

$$\nu_z = 2$$
$$\nu_x + \nu_z = 4.$$

strong imperfection resonances, so no statements can be made about the above inherent resonances. No other fourth integral resonances are observed including the difference resonance $2\nu_x - 2\nu_z = 0$.

There appear to be no signs of any higher order resonances. The above results, including the lack of any difference resonances, are similar to those of the Brookhaven group and are in good agreement with the predictions of the theories by Moser[9] and Sturrock.[10]

ACKNOWLEDGMENTS

We wish to thank D. W. Kerst for his great help and enthusiastic support throughout the entire course of this investigation.

It is also a pleasure to acknowledge the very great contributions made by L. J. Laslett, H. K. Meier, E. Rowe, R. P. Scharenberg, A. M. Sessler, J. N. Snyder, M. Stewart and K. R. Symon. In addition, we would like to thank the many other members of the MURA technical group who have made significant contributions.

The accelerator was constructed at the University of Michigan in space provided by the Michigan Memorial Phoenix Project. The magnets were fabricated and tested at Purdue University and the University of Illinois. One of us (F.T.C.) desires to thank the University of Illinois for its hospitality during a portion of this work.

1 Symon, Kerst, Jones, Laslett & Terwilliger, Phys. Rev. 103, 1837 (1956)

2 A preliminary note is given by Jones, Terwilliger & Haxby, Rev. Sci. Instr. 27, 651 (1956).

3 Goldstein, Classical Mechanics, (Addison-Wesley, Cambridge, Mass, 1950)p. 233.

4 Wills, Vector and Tensor Analysis, (Prentice-Hall, New York, 1931)p. 56.

5 Whittaker and Watson, Modern Analysis, (Cambridge U. Press, Cambridge, and MacMillan, New York, 1946)p. 412.

6 This method is due to D. W. Kerst, MURA report FTC/DWK-1 (unpublished).

7 These methods are discussed in detail in MURA reports LJL(8), 205 and 211, (unpublished) by L. J. Laslett.

8 Hammer, Pidd and Terwilliger R.S.I. 26, 555 (1955).

9 J. Moser, Nach. Akad. Wiss. Göttingen, Math.-Physik Kl. IIa, No. 6, p. 87 (1955).

10 P. Sturrock, Static and Dynamic Electron Optics, (Cambridge U. Press, Cambridge, 1955) and A.E.R.E. X/R 1771 (Harwell, Berks., 1955) (unpublished).

11 E. D. Courant and H. S. Snyder - Brookhaven Report EDC/HSS-1 (unpublished).

12 A survey of a similar nature has been made with the Brookhaven AG electron analogue, Courant et al, Phys. Rev. 100, 1269(A) (1955) and E. D. Courant, Proceedings of the CERN Symposium on High Energy Accelerators and Pion Physics, Vol. 1. (CERN, Geneva, 1956)p. 257.

13 While difficulties have been anticipated near this line from digital computation experience with spiral sector accelerators (L. J. Laslett and K. R. Symon, Proceedings of the CERN Symposium on High Energy Accelerators and Pion Physics. Vol. 1., (CERN, Geneva, 1956)p. 279,) digital computation with the fields of calculation 1 of Sec. III have shown no instability, but only an exchange of amplitude between radial and vertical oscillations, with a maximum vertical amplitude well within the limits of the accelerator aperture.

Figure

1. Schematic plan view of the radial sector FFAG model showing a typical equilibrium orbit. The wide (positive-field) magnets are radially focusing and vertically defocusing. The narrow (negative-field) magnets are vertically focusing and radially defocusing.
2. Magnetic field and electron energy as functions of the machine radius in the center of a negative-field magnet.
3. Geometry of the equilibrium orbit.
4. Schematic cross section of a magnet and the vacuum chamber.
5. A positive-field magnet. A portion of the pole-face winding for the lower pole is visible.
6. Circuit diagram of the null reading flip coil arrangement used to determine the field gradient index of the magnets.
7. Photograph of the complete accelerator.
8. Photograph of the accelerator with one magnet removed to show a portion of the aluminum vacuum chamber and a port containing a probe. One of the insulated gaps in the aluminum table is visable as a dark line running across the table below the flange joining the two halves of the tank.

9.a. Circuit diagram of the expander used to prevent the beam from striking the injector.

b. Voltage waveform of the expander pulse. The relative timing of expander and injector pulses is indicated.

10. Effects of misalignments of individual magnets on the equilibrium orbit in the accelerator.

    a. Radial displacement of a wide magnet.

    b. Radial displacement of a narrow magnet.

c. Vertical displacement of a wide magnet.

d. Vertical displacement of a narrow magnet.

The ordinates of curves a and b are the differences between the displacements of the perturbed equilibrium orbits from the unperturbed equilibrium orbit at two diametrically opposite probes. The ordinates for curves c and d are the displacements of the perturbed equilibrium orbits from the unperturbed equilibrium orbit. Orbit displacements are in units of the magnet displacement. The positions marked on the abcissas represent the centers of straight sections between sectors. The curves are drawn through the calculated displacements (circles). Measured displacements are represented by squares.

11. Beam intensity as a function of current tuning ratio with no current through the Δk coils. Relative beam intensity as measured by the scintillation counter is plotted on a logarithmic scale. ν_x and ν_z of the points measured by the rf resonance method are indicated above the curve. Points of crossing of certain resonances are also indicated.

12. Beam intensity as a function of Δk current tuning at the fixed current ratio 1.10. Relative beam intensity is plotted versus the ratio of Δk current in the positive magnets to the main current in the positive magnets. ν_x and ν_z of the points measured by the rf resonance method are indicated above the curve along with certain resonances.

13. Resonance survey diagram. The region of the ν_x- ν_z stability diagram covered by the experimental survey is enclosed within the dotted lines. Lines of equal beam intensity are drawn for each factor of $\sqrt{10}$ in intensity. The outermost intensity line represents a pulse height of 0.1 volt while the number in the center of each region gives the maximum pulse height of

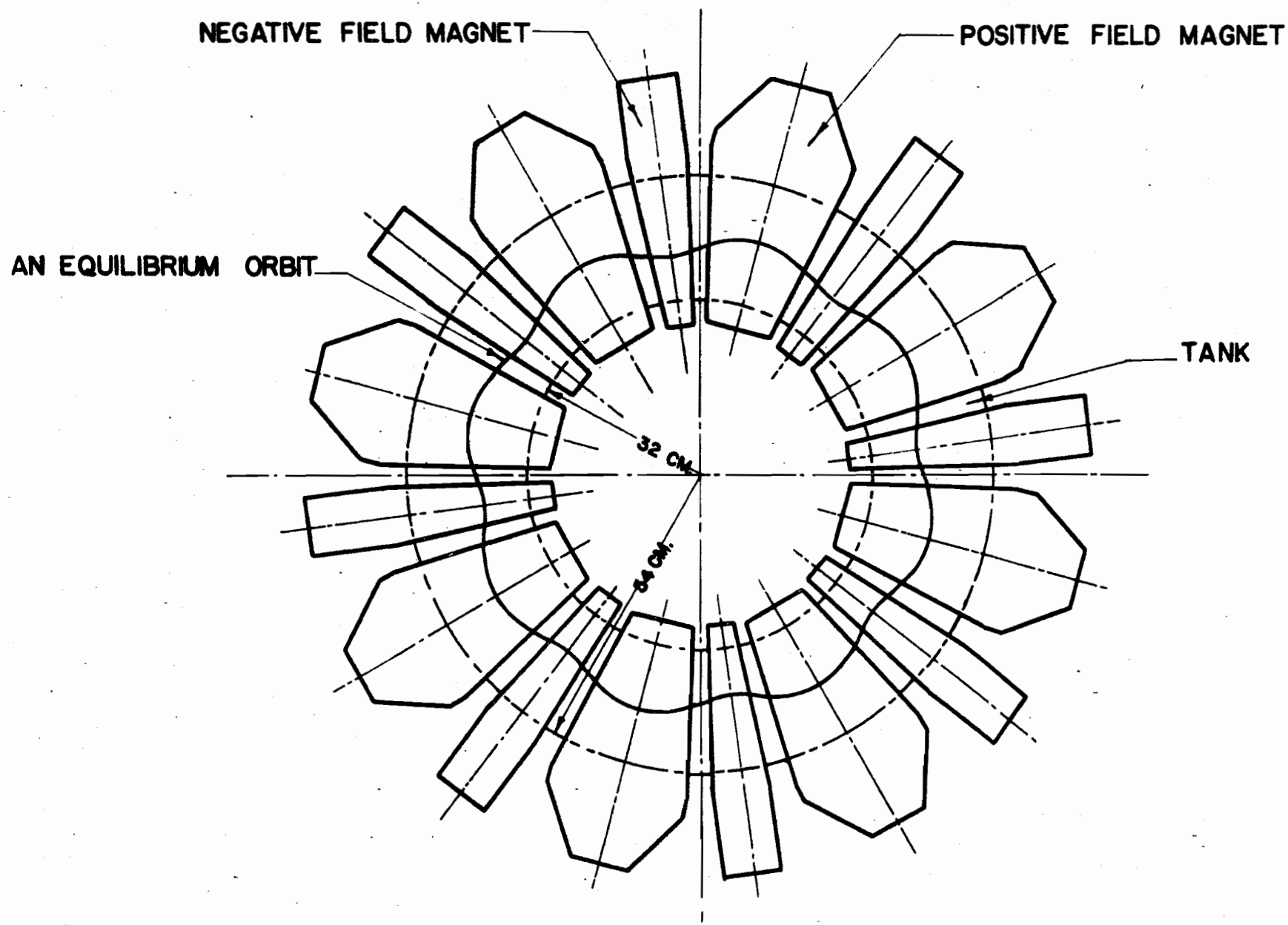
NEGATIVE FIELD MAGNET
POSITIVE FIELD MAGNET
AN EQUILIBRIUM ORBIT
TANK
32 CM.
64 CM.

Figure 1

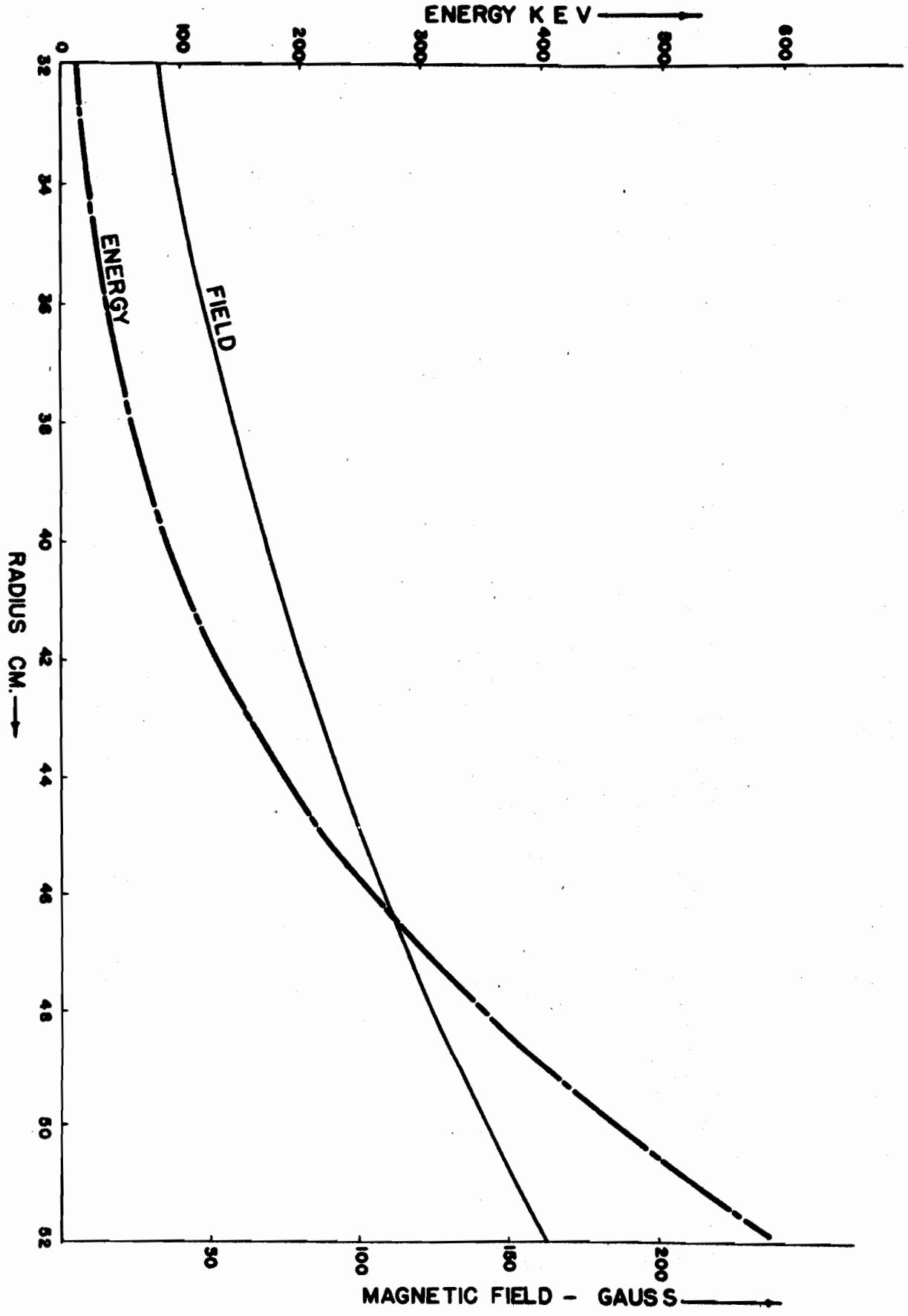
ENERGY K E V
0
100
200
300
400
500
600
32
34
36
38
40
42
44
46
48
50
52
RADIUS CM.
ENERGY
FIELD
50
100
150
200
MAGNETIC FIELD - GAUSS

Figure 2

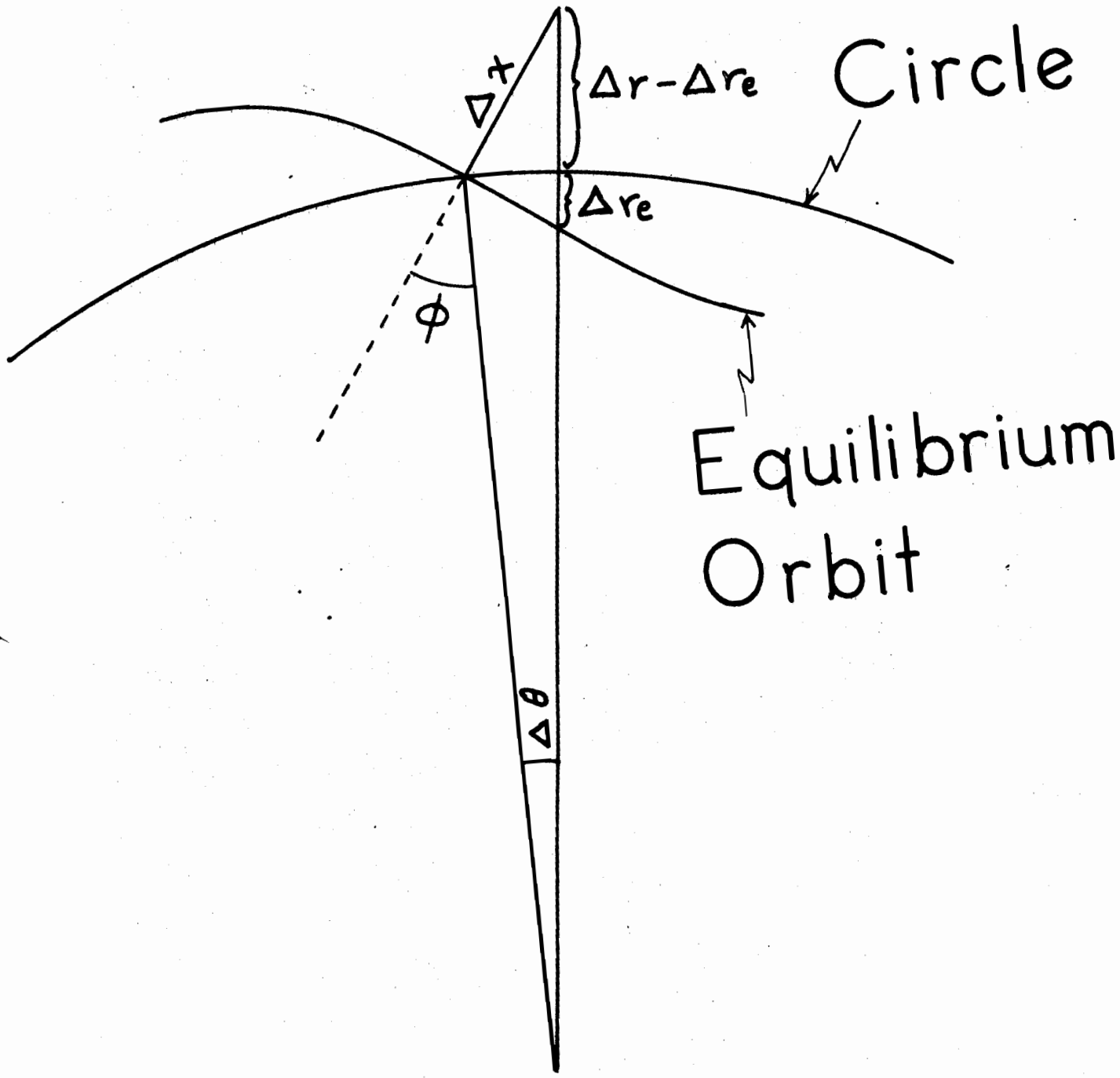
Δr^+
$\Delta r - \Delta r_e$
Circle
Δr_e
ϕ
Equilibrium
Orbit
$\Delta\theta$

Fig. 3

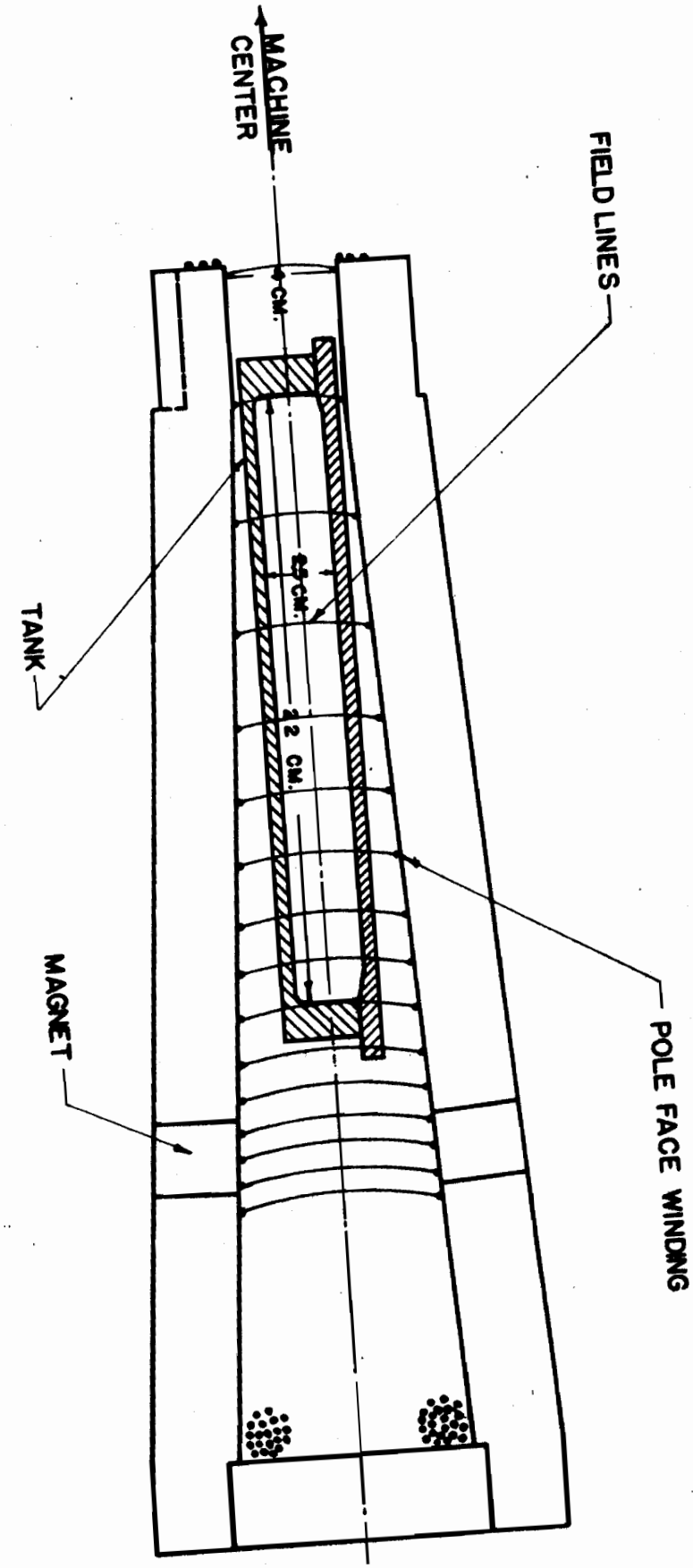
MACHINE CENTER
FIELD LINES
TANK
MAGNET
POLE FACE WINDING
CM.
CM.
CM.

Figure 4

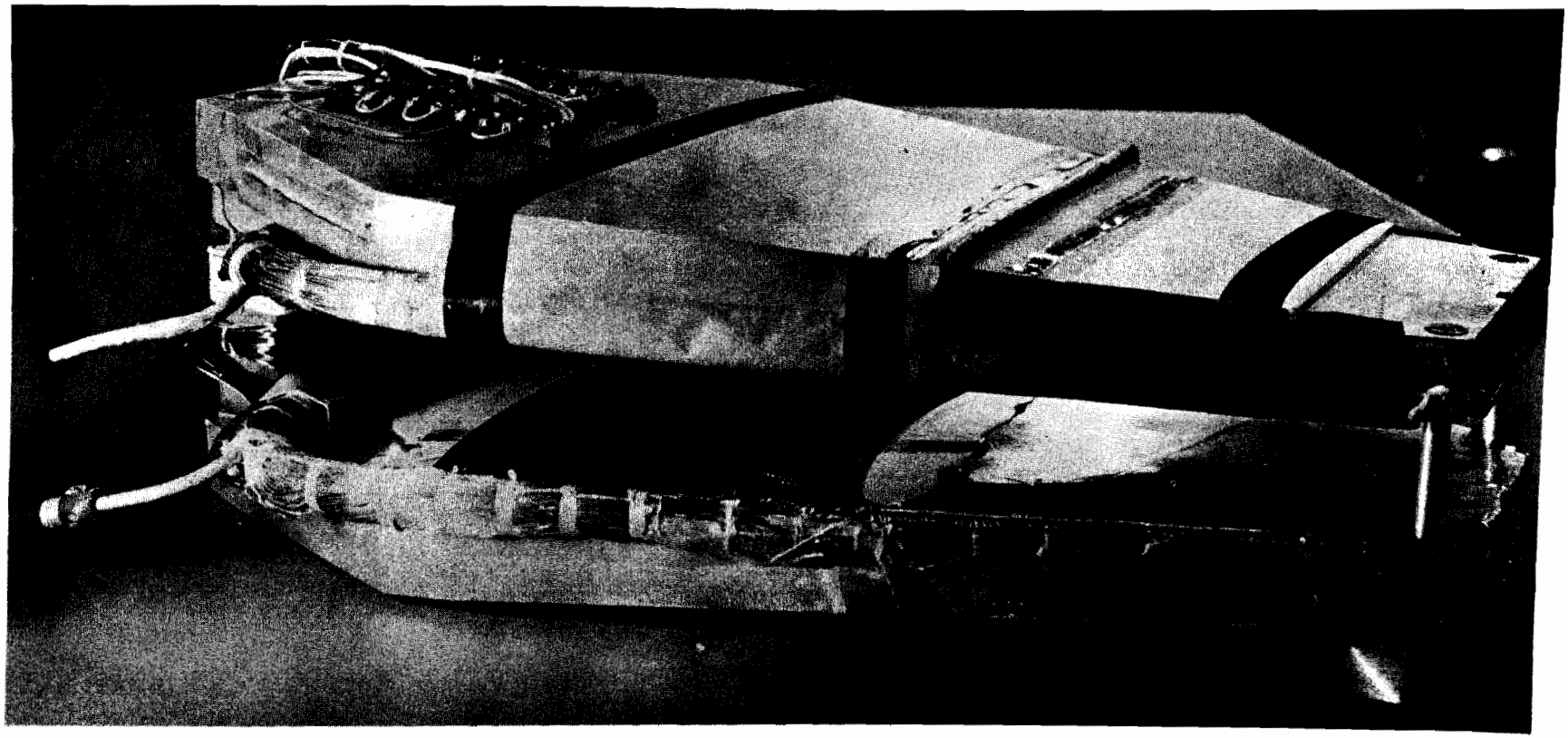

Fig. 5

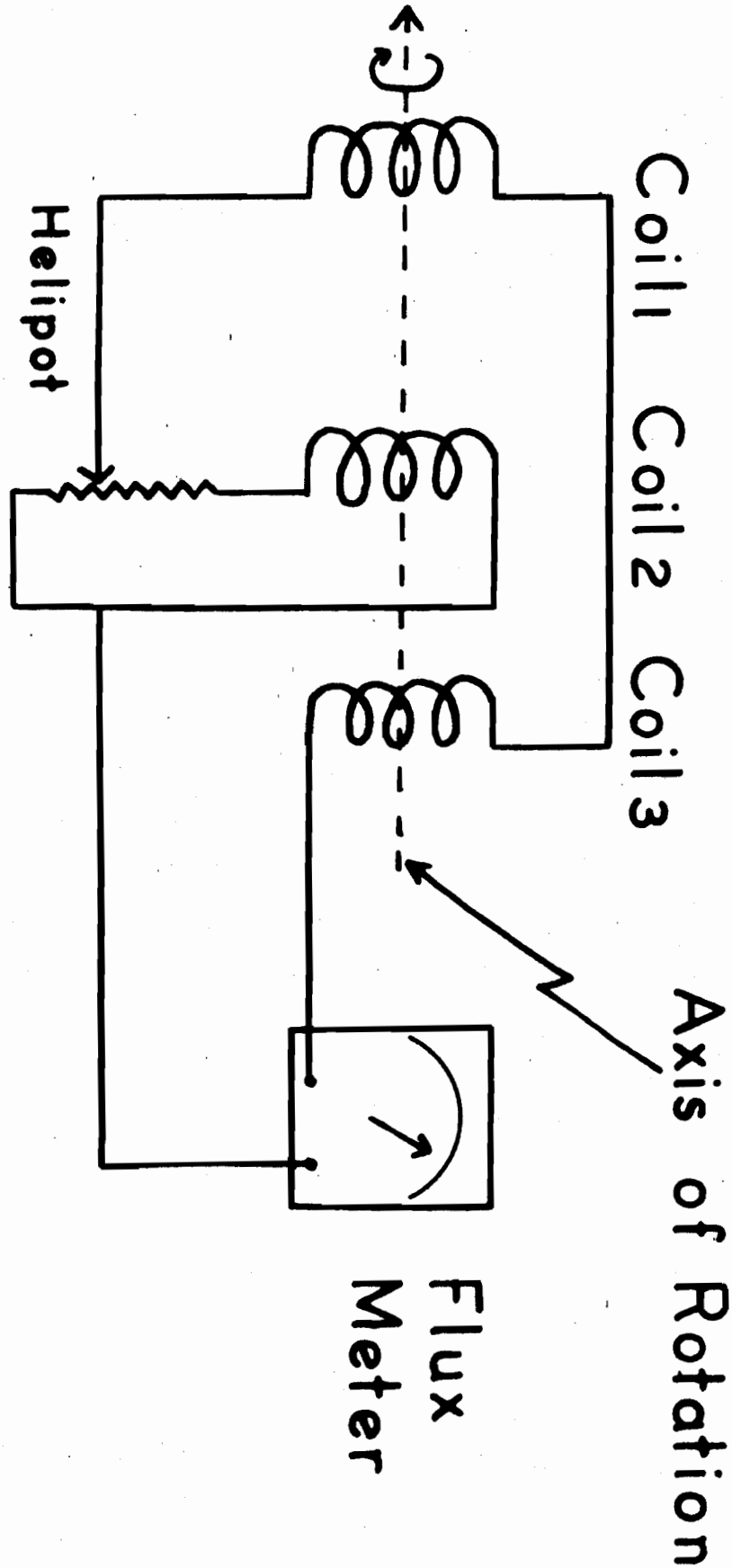

Figure 6

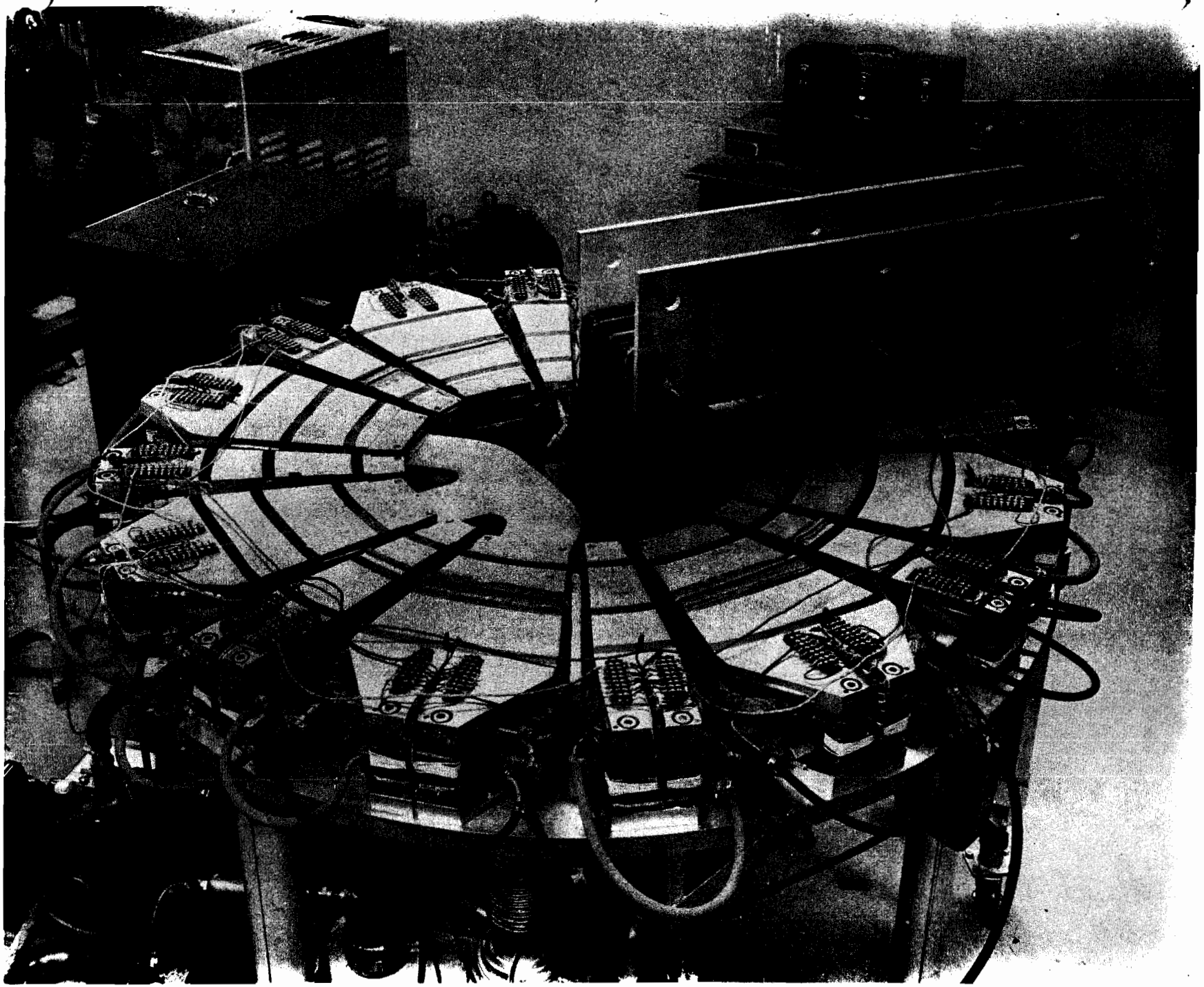

Fig. 7

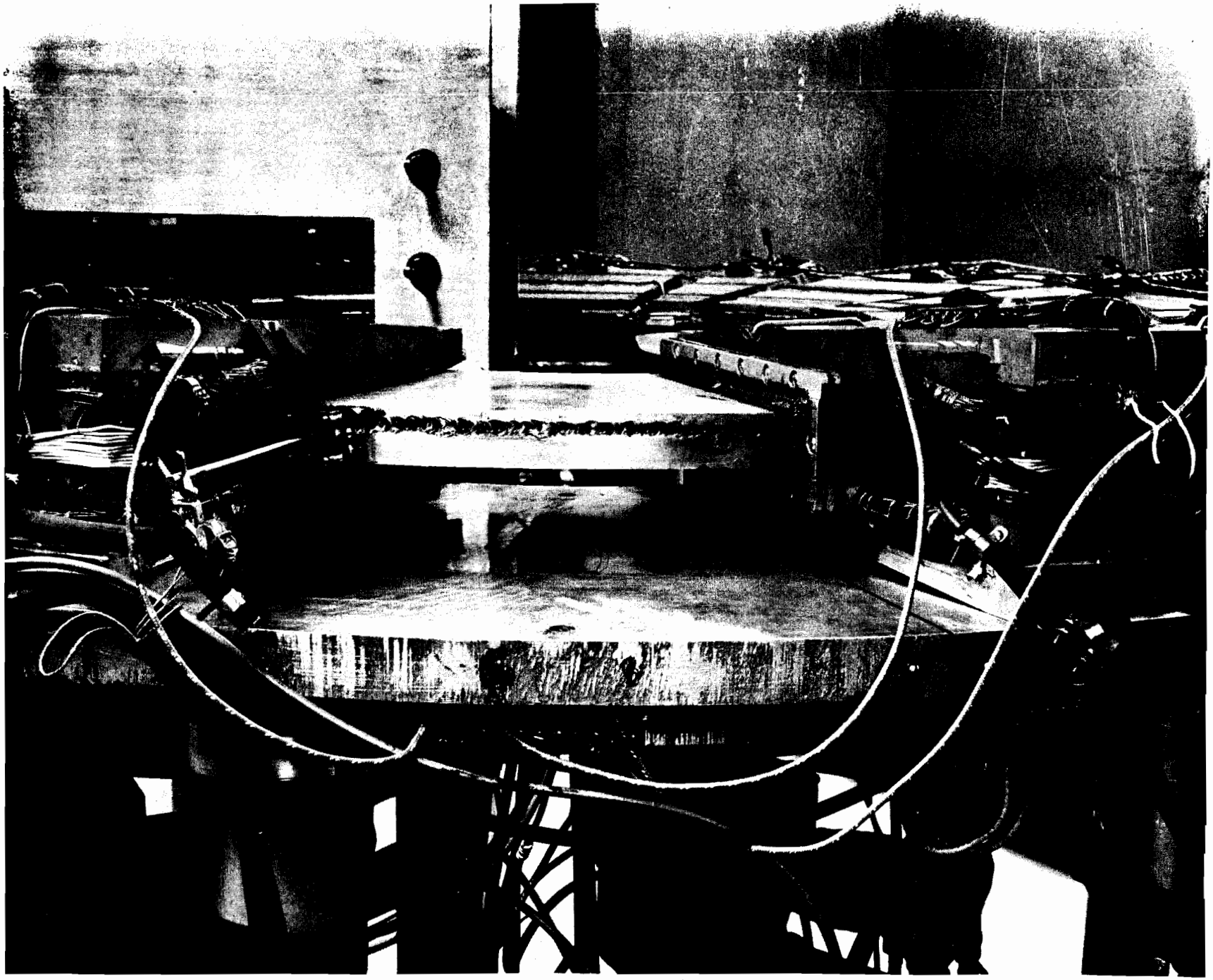

Fig. 8

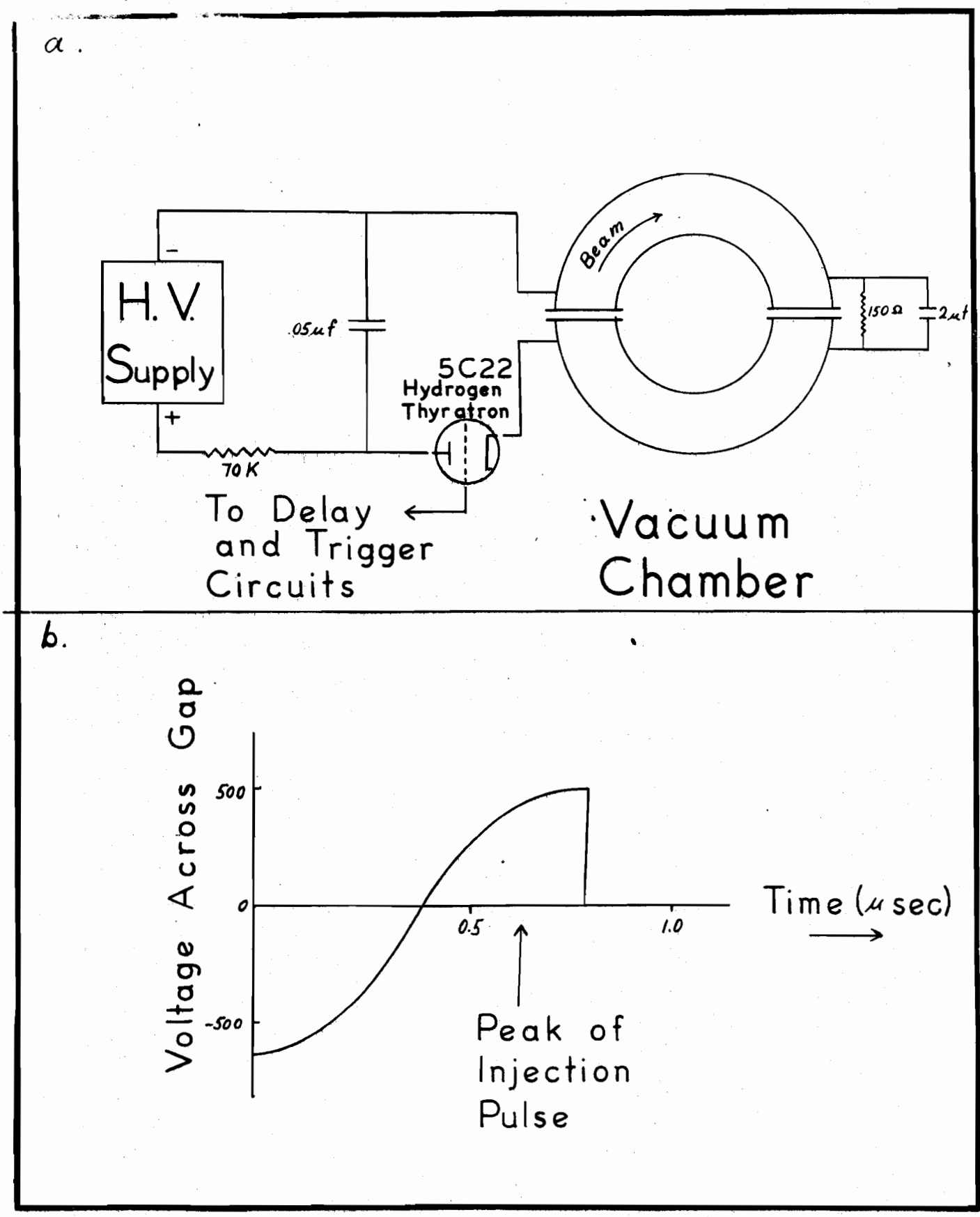
a.
H.V. Supply
-
+
.05μf
70K
5C22
Hydrogen
Thyratron
To Delay and Trigger Circuits
Beam
150Ω
2μf
Vacuum Chamber
b.
Voltage Across Gap
500
0
-500
0.5
1.0
Time (μsec)
Peak of Injection Pulse

Fig. 9

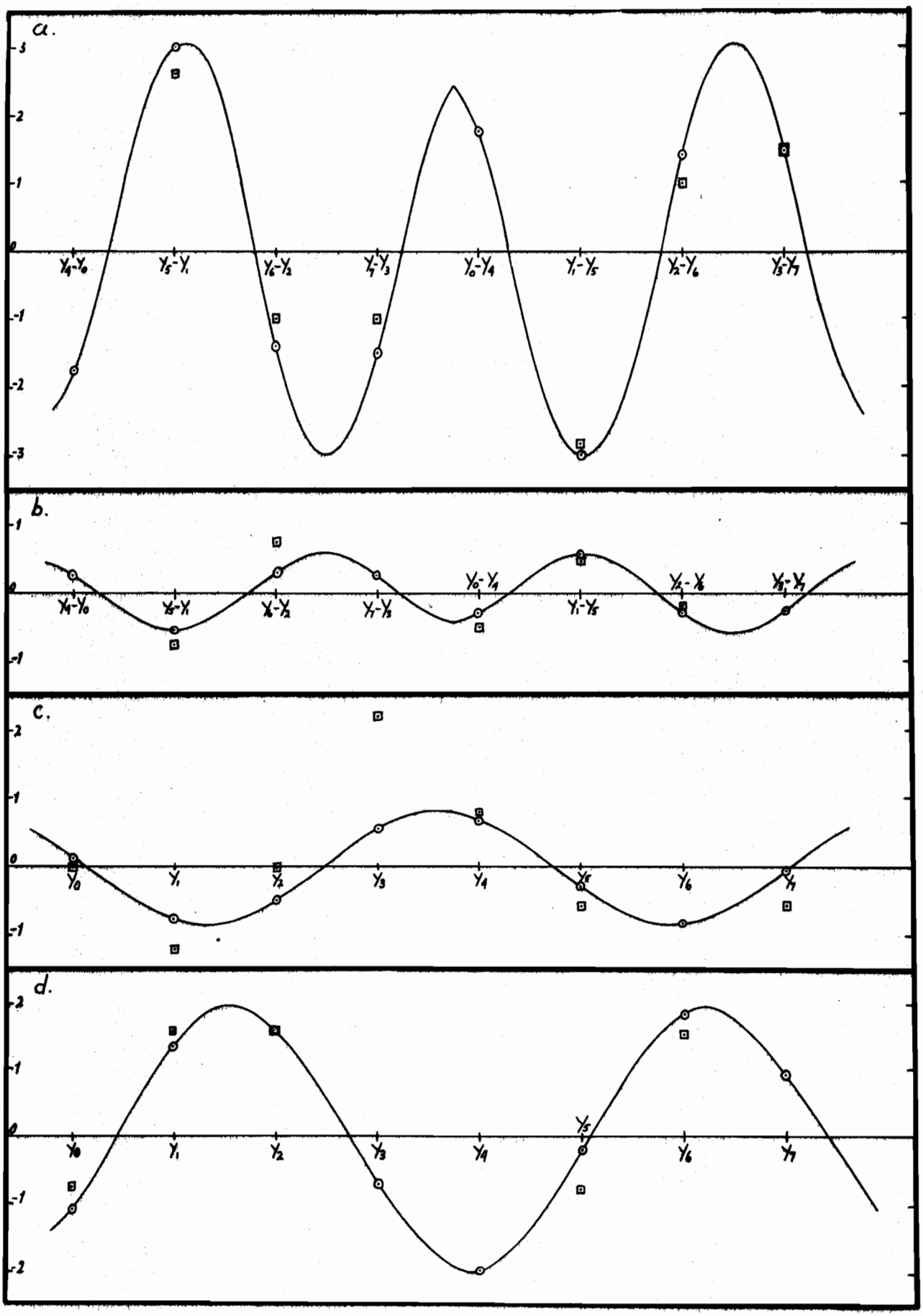

Fig. 10

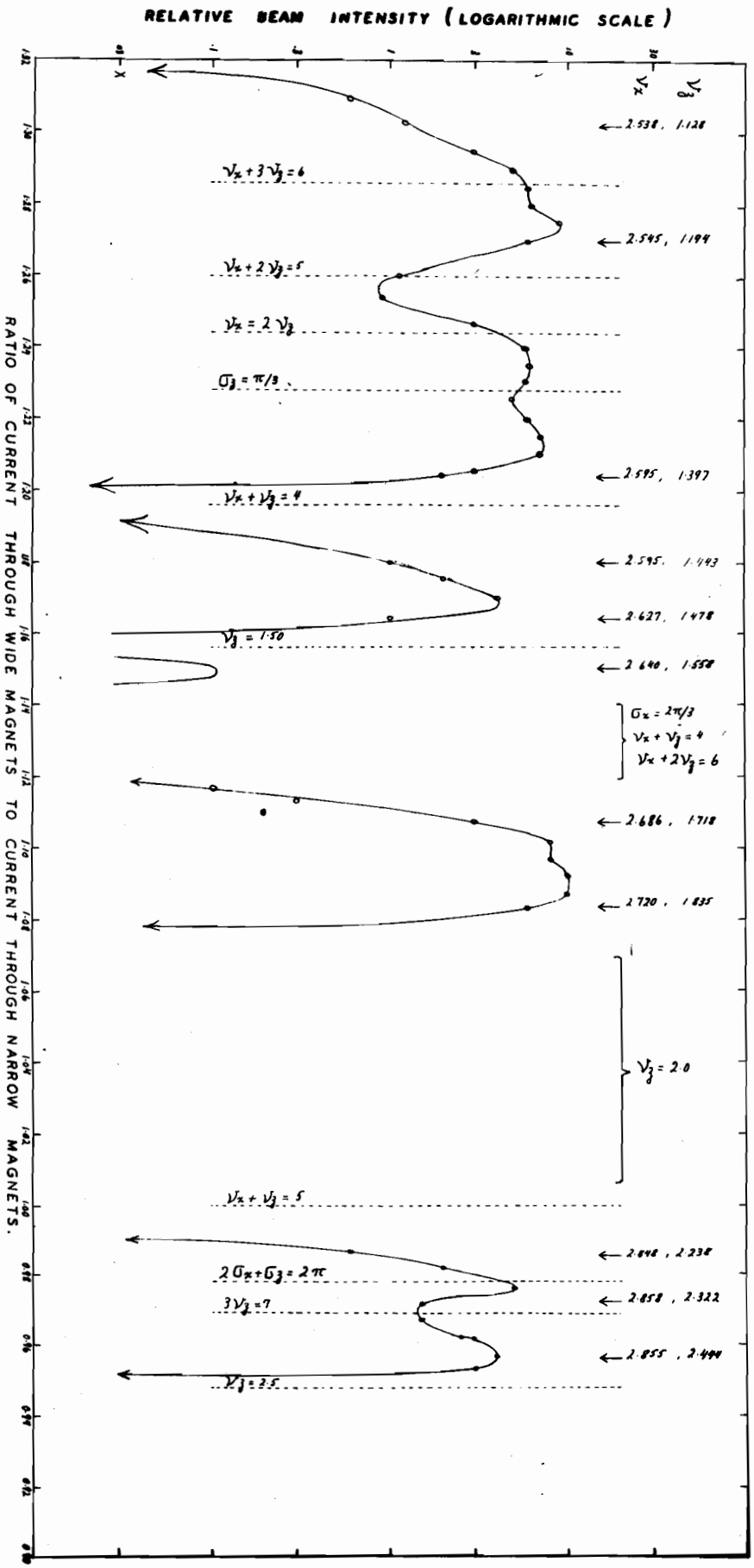
RELATIVE BEAM INTENSITY (LOGARITHMIC SCALE)
RATIO OF CURRENT THROUGH WIDE MAGNETS TO CURRENT THROUGH NARROW MAGNETS.
ν_x
ν_y
2.538, 1.128
$\nu_x + 3\nu_y = 6$
2.545, 1.194
$\nu_x + 2\nu_y = 5$
$\nu_x = 2\nu_y$
$\sigma_y = \pi/3$
2.595, 1.397
$\nu_x + \nu_y = 4$
2.595, 1.493
2.627, 1.478
$\nu_y = 1.50$
2.640, 1.558
$\sigma_x = 2\pi/3$
$\nu_x + \nu_y = 4$
$\nu_x + 2\nu_y = 6$
2.686, 1.718
2.720, 1.835
$\nu_y = 2.0$
$\nu_x + \nu_y = 5$
2.848, 2.238
$2\sigma_x + \sigma_y = 2\pi$
$3\nu_y = 7$
2.858, 2.322
2.855, 2.494
$\nu_y = 2.5$

Fig. 11

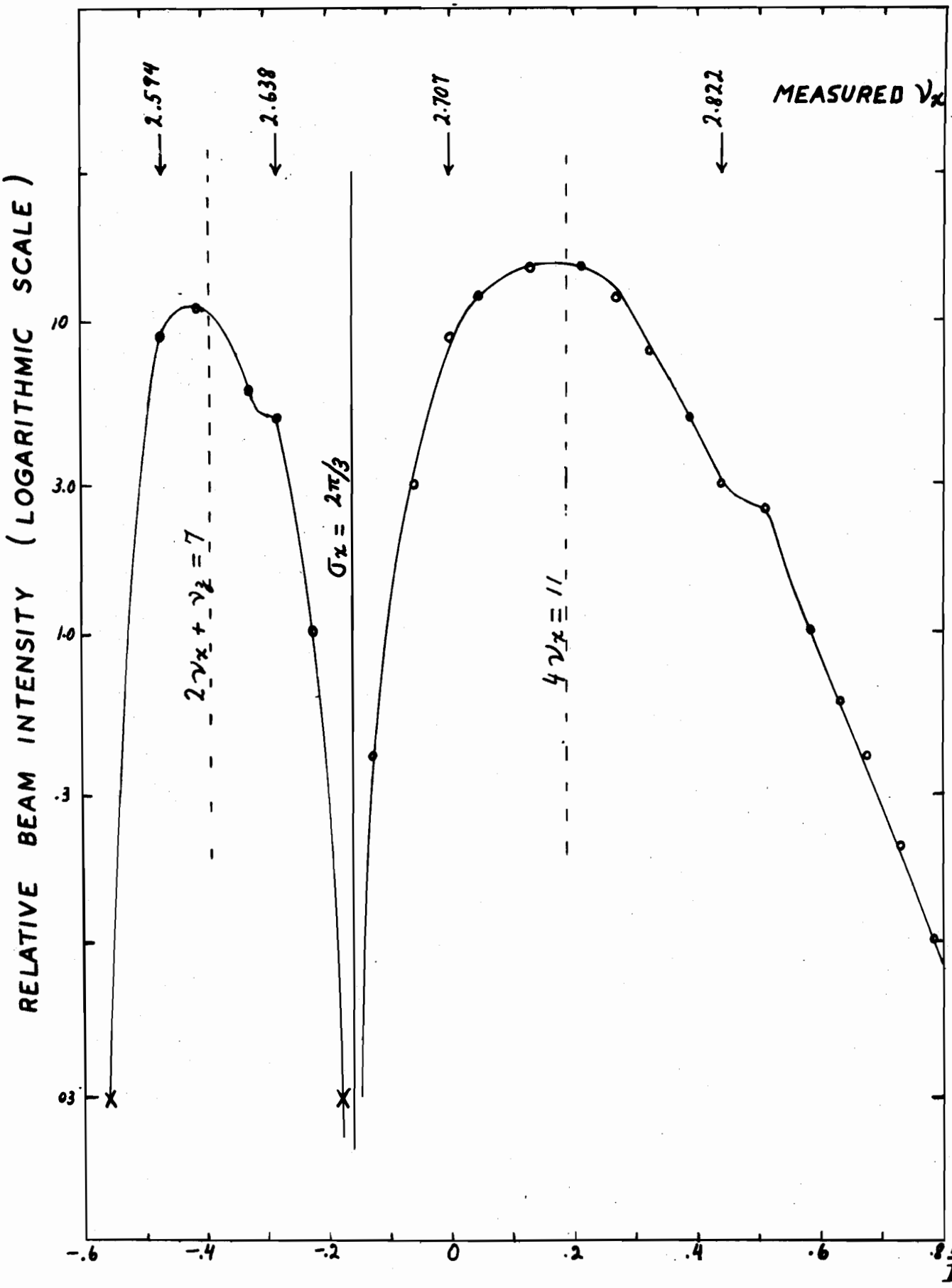
RELATIVE BEAM INTENSITY (LOGARITHMIC SCALE)
MEASURED ν_x
2.594
2.638
2.707
2.822
$2\nu_x + \nu_z = 7$
$\sigma_x = 2\pi/3$
$4\nu_x = 11$
10
3.0
1.0
.3
.03
-.6
-.4
-.2
0
.2
.4
.6
.8
$\frac{I_+}{I_+}$

Fig. 12

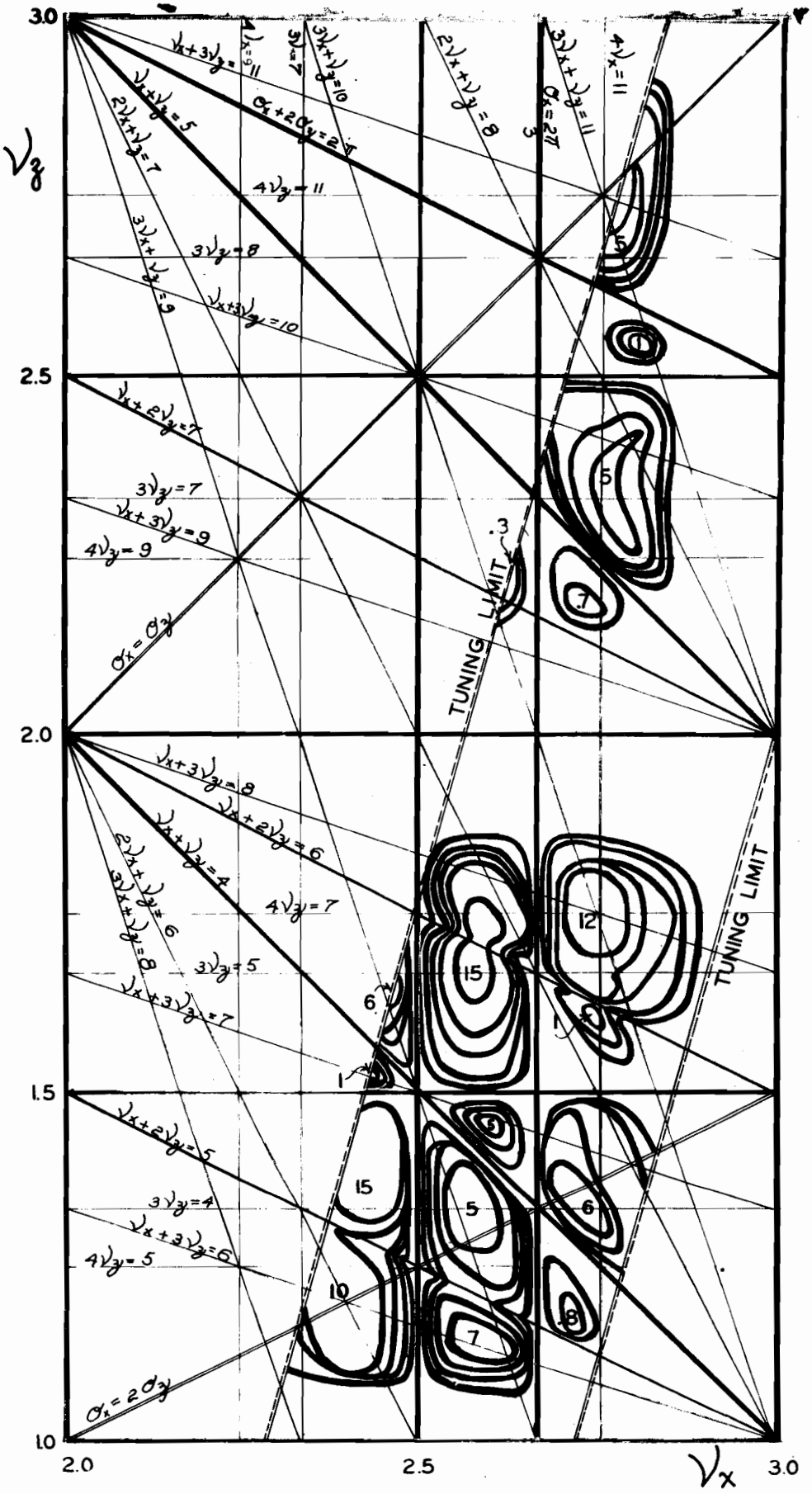
3.0
2.5
2.0
1.5
1.0
2.0
2.5
3.0
ν_y
ν_x
$\nu_x+3\nu_y=11$
$3\nu_x+\nu_y=10$
$\nu_x+2\nu_y=8$
$3\nu_x+\nu_y=11$
$4\nu_x=11$
$\nu_x+3\nu_y=7$
$\nu_x+\nu_y=5$
$2\nu_x+\nu_y=7$
$\sigma_x+2\sigma_y=27$
$4\nu_y=11$
$3\nu_y=8$
$3\nu_x+\nu_y=9$
$\nu_x+3\nu_y=10$
$\nu_x+2\nu_y=7$
$3\nu_y=7$
$\nu_x+3\nu_y=9$
$4\nu_y=9$
$\sigma_x=\sigma_y$
TUNING LIMIT
$\nu_x+3\nu_y=8$
$\nu_x+2\nu_y=6$
$\nu_x+\nu_y=4$
$2\nu_x+\nu_y=6$
$3\nu_x+\nu_y=8$
$4\nu_y=7$
$3\nu_y=5$
$\nu_x+3\nu_y=7$
TUNING LIMIT
$\nu_x+2\nu_y=5$
$3\nu_y=4$
$\nu_x+3\nu_y=6$
$4\nu_y=5$
$\sigma_x=2\sigma_y$
15
12
6
1
15
5
6
10
8
7

Fig. 13